Biointerface Research in Applied Chemistry
Open-Access Journal (ISSN: 2069-5837)

Article
Volume 13, Issue 4, 2023, 387
https://doi.org/10.33263/BRIAC134.387

Newly Modified Nanoformulation of Quercetin as Promising Chemotherapeutic Anticancer Agent

Mohamed El-Far [1,*], Alaa Essam [1], Fardous F. El-Senduny [1], Amira O. Abd El-Azim [2], Sarah Yahia [3], Ibrahim M. El-Sherbiny [3,*]

1 Biochemistry Division, Faculty of Science, Mansoura University, 35516, Egypt
2 Zoology Department, Faculty of Science, Mansoura University, 35516, Egypt
3 Nanomedicine Research Labs, Center for Materials Science (CMS), Zewail City of Science and Technology, 6th October City, 12578 Giza, Egypt
* Correspondence: elfarma2002@yahoo.com; (M.E.); ielsherbiny@zewailcity.edu.eg; (I.E.);

Scopus Author ID 8681880000
Received: 12.07.2022; Accepted: 26.08.2022; Published: 31.10.2022

Abstract: Previous studies have demonstrated the potential anticancer effect of quercetin (QUR). However, water insolubility and less bioavailability of QUR reduce its efficiency in cancer therapy. So, this study aims to develop a nanoformulation of quercetin (QURnp) and evaluate its anticancer effect against Ehrlich ascites carcinoma (EAC)-bearing mice compared with native QUR. QUR- loaded pluronic nanoparticles (QURnp) were prepared and characterized. To investigate the anticancer effect of QUR and QURnp, histopathological, ultrastructural, immunohistochemical, cell cycle analysis, western blot, and qRT-PCR studies were performed on EAC tumor cells, as well as antioxidant biomarkers. The results showed that QURnp destroyed tumor cells and significantly elevated antioxidant status with the reduction in MDA and NO levels. QURnp caused mitochondrial degeneration in tumor cells. Furthermore, QURnp completely reduced tumor growth by inhibiting the IL-6/STAT3 signaling pathway, inducing cell cycle arrest at the G1/S phase via overexpression of p27 and suppression of angiogenesis via downregulation in VEGF gene expression. Moreover, immunohistochemical studies indicated that QURnp showed significant inhibition of proliferation marker Ki-67 and anti-apoptotic marker Bcl-2. This study demonstrated that QURnp is a promising anticancer agent superior to native QUR.

Keywords: Quercetin; anticancer; pluronic nanoparticles; EAC; IL-6/STAT3; VEGF; mitochondria; cancer.

1. Introduction

The growth of cancer around the world has guided us to look for novel therapeutic drugs which are toxic to the tumor cells without adverse effects on healthy cells. Where the currently used anticancer drugs showed high toxicity to the tumor cells and to the normal cells of the body as well [1], so natural products from different plants, also called phytochemicals, act as crucial sources for cancer therapy by improving treatment efficiency in cancer patients and decreasing unfavorable reactions [2]. Phytochemicals such as polyphenols and flavonoids have been exhibited to have promising anticancer activities against a wide range of cancers [3,4].

Quercetin (QUR) (3,3′,4′,5,7- pentahydroxy-flavone), QUR, is the major flavonoid in vegetables and fruits and has antioxidant, anti-inflammatory, and anticancer activities. Quercetin can be utilized to protect the body against many diseases because of its ability to

scavenge free radicals [5,6]. Additionally, quercetin can suppress various types of cancer [7-10]. It has been found that quercetin is safe for normal cells. However, it has cytotoxic effects on tumor cells via various mechanisms [7]. Briefly, it can exhibit antitumor effects by inducing cell cycle arrest, promoting apoptosis, inhibiting cell proliferation, and suppressing angiogenesis and metastasis [11].

Besides several advantages of quercetin as an anticancer agent, it has different limitations for its *in vivo* application, such as chemical instability, poor absorption, bioavailability, and rapid systemic elimination. So, nanomedicine is the best way to develop novel formulations for hydrophobic drugs and may therefore overcome these limitations [12,13]. Furthermore, there are various types of nanocarriers have been conjugated with anticancer herbal bio-actives to overcome the problem of hydrophobicity [14]. The encapsulation of anticancer drugs into nanoparticles has displayed the ability to improve their solubility stability, prolong circulation time, and enhance tumor targeting [15]. So, nanoparticles-delivered QUR represents a valuable option to enhance its anticancer properties by increasing solubility, bioavailability, and short half-life lead to be accumulated in tumor site through enhanced permeability and retention (EPR) effect [16-18].

Our previous studies have shown that the entrapment of anticancer agents such as silymarin and curcumin into pluronic nanocarrier could improve their anticancer properties and promote their uptake efficiency as well as cytotoxicity in cancer cells which are found to be a good candidate for drug delivery [19,20]. Pluronic polymers are a special class of synthetic block copolymers that have been approved (US FDA). Pluronics are an excellent biological material for drug delivery because of their superior amphiphilic and biocompatibility properties, which could enhance circulation time and accumulation of drugs in tumor sites [21,22].

In the current study, we aimed to prepare a newly modified nanoformulation of QUR and investigate the antitumor effect of QUR-loaded pluronic nanoparticles (QURnp) as an ideal promising nanoformulation for cancer therapy as well as compare its mechanism of action with free quercetin.

2. Materials and Methods

2.1. Chemicals and drugs.

Quercetin (QUR), a pure yellow powder with a chemical formula of $C_{15}H_{10}O_7$ and MW of 302.24 g/mol, was purchased from Sigma-Aldrich (St. Louis, MO, USA). Pluronic F-108 (MW 14,600 g/mol) and pluronic F-127 (MW 12,600) were purchased from Sigma-Aldrich (Germany). Acetone 99.9% and all other solvents and used reagents were in a high analytical grade.

2.2. Preparation of plain and QUR-loaded nanoparticles.

The plain and QUR-loaded pluronic nanoparticles (QURnp) were prepared *via* the nanoprecipitation method [23]. The superior, pluronic type (F-127 and F-108), polymer-to-drug ratio, and also the organic-to-aqueous phase volume ratio were chosen based on many trials measuring the size, drug entrapment efficiency (EE%), and the drug loading capacity (LC%). In brief, the drug (QUR) was added to pluronic (F-127) in a ratio of 1:2 (drug: total polymer). Particularly, 50 mg of the drug and 100 mg of pluronic (F-127) were dissolved in 5 ml acetone. Then, the QURnp was obtained by adding this solution dropwise into 7.5 ml de-

ionized water with continuous stirring at 250 rpm till the formation of nanosuspension. To optimize the size of the resulting nanoparticles NPs, pluronic F-108 was used at the same ratio by dissolving 50 mg of the drug (QUR) and 100 mg of F-108 in 5 and 10 ml acetone, respectively, followed by mixing the two solutions. The QUR/F-108 acetone solution was poured dropwise on 40 ml de-ionized water, and the size of the resulting nanosuspension was measured. Besides, QURnp of ratio 1:3 drug : polymer (F-108) was prepared. Particularly, a drug (QUR) solution of 50 mg in 5 ml acetone and pluronic F-108 solution of 150 mg in 10 ml acetone were prepared and mixed, followed by their dropwise addition to 40 ml de-ionized water. Afterward, all the NPs developed using different types of pluronic (F-127 and F-108) and different drug-to-pluronic ratios (1:2 and 1:3) were subsequently frozen at -80^{o}C followed by freeze-drying (FreeZone 6, Labconco) at -50^{o}C for 24 h, and then stored at 4^{o}C for further investigations. The plain (QUR-free) NPs were fabricated by the same procedure and used as the control.

2.3. Characterization of plain and QUR-loaded nanocarriers.

The size and zeta potential of the prepared plain (QUR-free) and QUR-loaded nanomicelles (QURnp) were measured by using Zetasizer (Malvern Instruments Ltd., Worcestershire, UK). Furthermore, transmission electron microscopy (TEM-JEOL, JEM-1230, Tokyo, Japan) at an accelerating voltage of 200 kV was used to examine the size and shape of produced nanomicelles. Fourier transform infrared spectroscopy (FTIR-Thermo Scientific) was used for the three components (QUR, plain, and QURnp) to examine each characteristic's peaks. FTIR was used in the range of 600−4000 cm^{-1}/ 25°C.

2.4. In-vitro biodegradation study.

The biodegradation experiment was carried out by diffusing 0.5 mg of the prepared pluronic NPs (F-108) in 0.4 ml PBS buffer (pH 7.4) containing lysozyme (1.4 mg/ml PBS, pH 7.4) following the protocol described earlier [23].

2.5. Determination of drug entrapment efficiency and loading capacity.

During the preparation of QUR-loaded nanomicelles (QURnp), the NPs suspension was centrifuged at 30,000 xg and 5^{o}C. Then, the aliquot was separated from the pellets to measure the concentration of the free drug using UV-Vis spectrophotometry at a wavelength of 320 nm. Both entrapment efficiency (EE %) and loading capacity (LC%) were calculated using the following equations:

$$EE\% = \frac{m_t - m_{un}}{m_t} \times 100 \qquad (1)$$

$$LC\% = \frac{m_l}{m_l + m_p} \times 100 \qquad (2)$$

where m_t, m_{un}, and m_l are the total amount, unloaded amount, and loaded amount of drug (mg), respectively. The m_p refers to the total weight of the pluronic polymer.

2.6. In-vitro drug release study.

Drug release was measured by suspension of either free drug or drug-loaded NPs (QURnp) in 2 ml of release solution (PBS pH 7.4 : acetone, 7:3) in a dialyzing membrane with 14 kDa cut-off. Then, the dialysis bag was immersed in 10 ml of the same solution that worked as a receptor media. The system was incubated in a shaker incubator at 37°C and 120 rpm

(VWR® incubating orbital shaker, VWR International, CA, USA). At pre-determined periods, 1 ml of aliquots were withdrawn and substituted with 1 ml of fresh release solution. All samples were tested using a UV-Vis spectrophotometer. The cumulative release of the drug (QUR) was obtained by using the following equation:

$$Cn = Cn\ means + \frac{A}{V}\sum_{s=1}^{n-1} Cs\ means \quad (3)$$

where Cn is the drug concentration according to the order of the sample, Cn means it is the examined concentration, A is the volume of the aliquot, V is the volume of the sink medium, n-1 is the sum of all previously withdrawn aliquots, and Cs is the sum of all previous aliquots' concentrations.

2.7. Animals and tumor model.

Female Swiss albino mice (20-25 g) were provided by VACSERA, Giza, Egypt. Mice were housed under standard laboratory conditions for 1 week and were given a standard diet and water ad libitum.

The experimental protocol was approved by University Animal Ethical Committee (Code no. Sci-Ch-ph-2022-168).

Mice were divided into 8 different groups (n=10). All mice in each group were injected intraperitoneally with EAC cells (1×10^6viable EAC cells/mouse/0.2 ml). Figure 1 explains the experimental design of the current study [19,20].

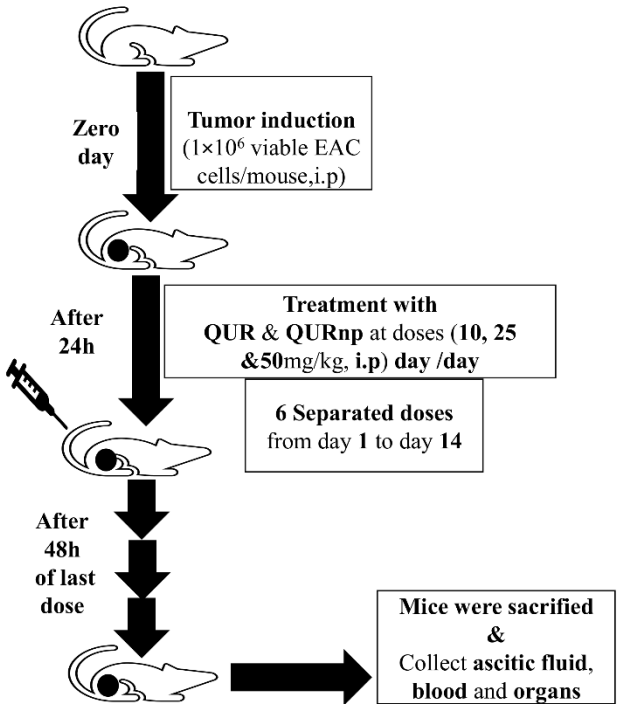

Figure 1. The experimental design of the current study.

2.8. Experimental design.

Group (1): Mice without any treatment as a control group.

Group (2): Mice were administrated i.p with 5% DMSO/saline as vehicle 1.

Group (3): Mice were administrated i.p with saline as vehicle 2.

Group (4): Mice were treated with (10 mg/kg body weight (b.wt), i.p) of QUR in 5% DMSO/ saline.

Group (5): Mice were treated with (25 mg/kg b.wt, i.p) of QUR in 5% DMSO/ saline.

Group (6): Mice were treated with(50 mg/kg b.wt, i.p) of QUR in 5% DMSO/ saline.
Group (7): Mice were treated with (10 mg/kg b.wt, i.p) of QURnp, in saline.
Group (8): Mice were treated with (25 mg/kg b.wt, i.p) of QURnp, in saline.
Group (9): Mice were treated with (50 mg/kg b.wt, i.p) of QURnp in saline.

2.9. Determination of tumor volume and viability percentage.

Ascetic fluid was collected from the peritoneal cavity of mice. Tumor volume was determined as well as viability percentage by Trypan blue exclusion method [24].

2.10. Determination of in vivo antioxidant activity.

The homogenate of tumor cells, as previously described [19,20], was used for the estimation of glutathione GSH, superoxide dismutase (SOD), catalase (CAT), and lipid peroxidation biomarker (MDA) using assay kits from Biodiagnostic, Egypt. The amount of NO was also determined in the supernatant of ascetic fluid by Griess assay [25].

2.11. Evaluation of hematological parameters.

Collected blood was used to evaluate hemoglobin (Hb) content, red blood cell (RBC), and WBC count using standard procedures.

2.12. Histopathological studies.

All samples, including ascites, liver, kidney, and spleen for various examined groups, were gathered and submerged in 10% buffered formalin pH 7.2 for at least 24 hours to be processed to form paraffin blocks that were sectioned via microtome into 3-5 µm thick sections for further staining procedure. Finally, the prepared slides were examined via Olympus Bx 51 light microscope.

2.13. Ultrastructural studies.

Ehrlich ascites carcinoma samples were collected in a 0.1 M buffer of cacodylate with glutaraldehyde and paraformaldehyde, fixed in a mixture buffer of 0.1 M cacodylate containing 2 mM calcium chloride, 1% osmium tetroxide and 0.8% potassium ferricyanide. After that, samples were dehydrated to be embedded in resin capsules to be sectioned *via* ultramicrotome and mounted on copper grids. Specimen were stained with 8% uranyl acetate for 10 minutes and 1% lead citrate for 5 minutes, according to Reynolds, then were dried for 15 minutes before examination by JEOL JEM-2100 at 60 kV at EM Unit, Mansoura University, Egypt [26].

2.14. Cell cycle analysis.

After treatment with free QUR and QURnp, EAC cells were fixed with 70% ice-cold ethanol and then were incubated with PI based on the method of El-Far *et al.* [24]. EAC cells were analyzed by flow cytometry. The data were determined using BD FACSCCalibur™ Flow Cytometer (Becton Dickson, Mountain View, CA).

2.15. Western blotting.

EAC cells were lysed using RIPA buffer, including 1x protease and phosphatase inhibitors cocktail. Total protein was separated on SDS-PAGE and then transferred onto the

nitrocellulose membrane. Afterward, the nitrocellulose membrane was blocked with 3% BSA and then was with primary antibodies against p27 (1:4000, Cell Signaling Technology, Cat No. 2552T), STAT3 (1:1000, Cell Signaling Technology, Cat No. 9139T), and p-STAT3 (Tyr705) (1:2000, Cell Signaling Technology, Cat No. 9145T), then washed and incubated with rabbit or mouse secondary antibodies and normalized to *β*-Actin protein levels as control. Protein bands were visualized using an ECL substrate and visualized with The ChemiDoc MP Imaging System (Bio-Rad).

2.16. Immunoenzymatic assay.

IL-6 was estimated by ELISA assay. The ascitic fluid from the peritoneal cavity was centrifugated at 300 x g for 10 minutes, and the obtained supernatant was used for the IL-6 analysis [27].

2.17. RT real-time PCR.

RNAs were extracted from EAC cells using *GeneJET RNA Purification* Kit (Thermo scientific). For RT-PCR, The HiSenScript™ RH(-) cDNA Synthesis Kit was used to convert RNAs to cDNA. qRT-PCR products were detected with SYBR Green *(SensiFAST SYBR® Hi-ROX Kit)* with 20 µl reactions. The β-actin gene was included as an internal control. qPCR data were analyzed by the $2^{-\Delta\Delta Ct}$ method. PCR primers were listed in (Table S1).

2.18. Immunohistochemical studies.

EAC sections were mounted on charged slides for further detection of Ki-67 (Thermo Fisher Scientific, Cat No. MA5-14520) and Bcl2 (Thermo Fisher Scientific, Cat No. MA5-11757) antibodies. Slides were washed 3 times using phosphate-buffered saline (PBS) and H_2O_2 to eliminate endogenous peroxidase activity. Next, blocking sections were with suitable blocking buffer, then removed the blocking solution followed by incubation with primary antibody overnight at 4°C; after that, sections were treated with secondary antibody and then stained with chromogen. Finally, Mayer's hematoxylin was used as a counterstain [28].

2.19. Ki-67 & Bcl2 immunostaining scoring approach.

For Ki-67 scoring, the percentage of positively stained nuclei to the whole cells in the field was assessed. In contrast, Bcl-2 scoring was detected in the brown-stained cytoplasm surrounding the nuclear membrane of positive cells. Counting was performed among 5 fields, and counts below 5% of positivity were counted negative [29].

2.20. Statistical analysis.

The present data were analyzed using the GraphPad Prism package, version 5.0 (GraphPad Software, CA, USA), and SPSS software, version 26.0 of One-Way ANOVA, to evaluate the significance and variance between groups. Data were expressed as mean ± SE (standard error). P-value < 0.05 was considered significant, $p<0.01$ was considered highly significant, and $p<0.001$ was considered extremely significant.

3. Results

3.1. Development and characterization of the plain and QUR-loaded nanomicelles (QUR-NPs).

In the present study, QUR was incorporated at different ratios into various pluronics (F-127 and F-108)-based nanocarriers to enhance the QUR aqueous solubility and increase its bioavailability. The QUR nanoformulation was also carried out to allow lower doses of the drug in the treatment protocol to avoid adverse side effects. This study also assesses the efficacy of the developed QUR-loaded nanoparticles (QURnp) as potential antitumor agents compared to the free drug (QUR) in EAC tumor-bearing mice as an experimental model.

The QUR-loaded pluronic nanomicelles (QURnp) were obtained using the nanoprecipitation method [23]. Nanoprecipitation is an appropriate technique for nanoformulation and delivery of hydrophobic bioactive compounds such as the drug under investigation (QUR). Besides, incorporating the sparingly-soluble drug (QUR) into nano-sized polymeric carriers enhances its solubility and bioavailability.

Table 1 shows the average size and zeta (ζ) potential of both plain and QUR-loaded NPs (QURnp) fabricated using different types of pluronic (F-127 and F-108) at the different drug to pluronic ratios (1:2 and 1:3), as examined by Zetasizer. As can be noted from the table, the size of plain F-127-based NPs and plain F-108-based NPs is 161.0 ± 31 nm and 278.3 ± 35 nm, respectively, and their corresponding surface charge (ζ) is -15.7 ± 1.1 mV and -24.4 ± 5.5 mV, respectively. Incorporating the drug (QUR) into both types of pluronic led to an increase in the particle size and a reduction in the surface charge (ζ) of the resulting NPs. For instance, with maintaining the drug: pluronic ratio constant at (1:2), the size of F-127-based NPs increased significantly from 161.0 ± 31 nm to 343.9 ± 41 nm, with a reduction in the zeta potential (ζ) from -15.7 ± 1.1 mV to -27.1 ± 3.0 mV. In the case of F-108-based NPs (1:2), the particle size increased from 278.3 ± 35 nm to 313.6 ± 33 nm, with a reduction in the zeta potential (ζ) from -24.4 ± 5.5 mV to -49.3 ± 2.7 mV. Loading a less amount of drug relative to the polymer, as in the case of F-108-based NPs (1:3), attained a smaller particle size of 222.8 ± 6.7 nm with a zeta potential (ζ) of -45.96 ± 3.3 mV.

Transmission electron micrographs of plain and QUR-loaded pluronic F-108 NPs (QURnp) are demonstrated in Figure 2. As can be noted from the figure, both plain (Figure 2a) and QURnp particles (Figure 2b) are spherical shapes. Besides, the TEM micrographs have confirmed the measured mean particle size of the obtained plain and QUR-NPs as obtained using the TEM particle analysis software (NanoScope Analysis, Veeco Co, USA).

Figure 2c illustrates the FTIR spectra of the drug (QUR), plain pluronic F-108, and QUR-loaded pluronic PF-108 NPs (QURnp). As apparent from the figure, the characteristic FTIR bands for pluronic F-108 were weak and centered at 3545 cm^{-1}, assigned to the stretching OH group and intermolecular hydrogen bonds. Additionally, a sharp band was noted at 2,881 cm^{-1} that may be assigned to the symmetric stretching vibrations of the –(CH_2)– groups. Peaks centered around 1359.5 cm^{-1} and 1279 cm^{-1} correspond to the in-plane bending of OH and the C–O–C stretching. Peaks of ether group (-C-O) stretching are observed at 1100 cm^{-1} and 1059.7 cm^{-1}, and the C-C-O asymmetric stretching was determined at 961 cm^{-1} [30-36]. Quercetin (QUR) characteristic bands were observed at 3277.7 cm^{-1}, 1661.5 cm^{-1}, 1605.6 cm^{-1}, and 1510.6 cm^{-1} that result from O-H stretching, C=O stretching, and C=C stretching, respectively. Other characteristic peaks of QUR located between 1090.7 cm^{-1} and 1350 cm^{-1} may be attributed to the –OH phenolic [37-40]. The FTIR spectrum of the developed QUR-loaded

pluronic PF-108 NPs (QURnp) depicted most of the characteristic peaks of both the drug (QUR) and the plain pluronic F-108, which confirms the successful incorporation of the drug into the NPs.

Table 1. The average size and zeta potential (ζ) of both plain and QUR-loaded NPs (QURnp) fabricated using different types of pluronic (F-127 and F-108) at the different drug-to-pluronic ratios (1:2 and 1:3) in addition to the corresponding values of the drug entrapment efficiency (EE%), and loading capacity (LC%).

Pluronic Type (Drug : Pluronic)	Size (nm)	ζ potential (mV)	EE%	LC%
F-127	161.0 ± 31	-15.7 ± 1.1	-	-
F-108	278.3 ± 35	-24.4 ± 5.5	-	-
F-127 (1:2)	343.9 ± 41	-27.1 ± 3.0	98.79 ± 0.6	49.39 ± 2.1
F-108 (1:2)	313.6 ± 33	-49.3 ± 2.7	98.84 ± 0.3	49.42 ± 1.9
F-108 (1:3)	222.8 ± 6.7	-45.96 ±3.3	99.02 ± 1.0	33.01 ± 4.3

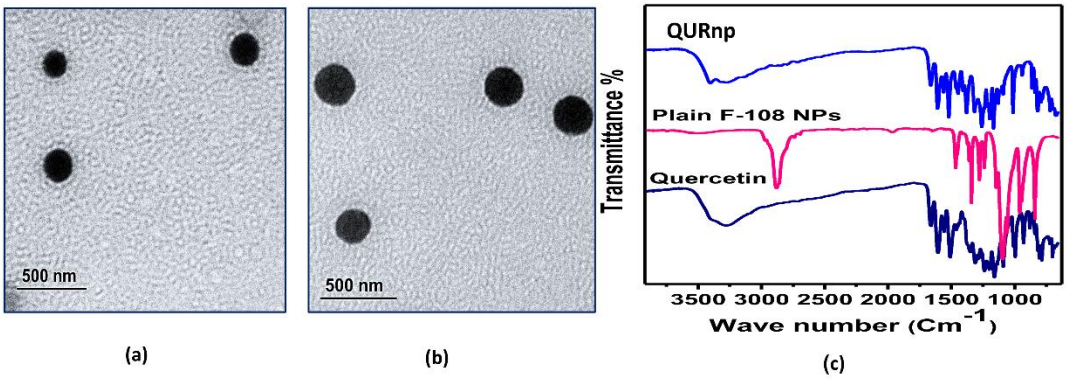

Figure 2. Transmission electron micrographs of **(a)** plain; and **(b)** quercetin-loaded pluronic PF-108 nanoparticles (QURnp) ; **(c)** FTIR spectra of quercetin (QUR), plain pluronic F-108, and quercetin-loaded pluronic F-108 nanoparticles (QURnp).

3.2. In vitro biodegradation and cumulative release studies.

An *in vitro* enzymatic degradation study of the plain pluronic F-108 nanocarrier was performed at 37ºC in PBS of pH 7.4 in the presence of lysozyme, as demonstrated in Figure 3a. The percent of weight loss of the polymeric nanocarrier as a function of time was determined and taken as a measure of biodegradation. As shown in (Figure 3a), the pluronic F-108 NPs have shown higher degradation rates in the presence of lysozyme. For example, the percent of degraded weights (Wd %) of the nanocarrier was almost 83.3 % after 2 days.

As can be noted from Table 1, the highest value of EE% of the drug (QUR) in the developed QURnp was 99.02 ± 1.0 % attained upon loading the drug (QUR) in pluronic F-108 nanocarrier at drug : polymer ratio of 1:3 with a corresponding LC% value of 33.01 ± 4.3%. Although this LC% value was the lowest as compared to the other developed two QUR-NPs; F-127 (1:2) and F-108 (1:2), it was chosen as the optimum nano formula in this study for further *in vivo* investigation due to the smaller NPs size (222.8 ± 6.7) and the higher EE% (99.02 ± 1.0 %).

(Figure 3b) shows the cumulative release profile of the free drug (QUR) and the drug from the developed QUR-loaded pluronic F-108 nanocarrier (QURnp) of QUR : polymer ratio of 1:3. It is obvious from the figure that the free (QUR) drug depicted a burst release up to 98% within 3 days. At the same time, the QUR-loaded NPs (QURnp) showed a sustained release that liberated around 78% of the drug (QUR) after 9 days.

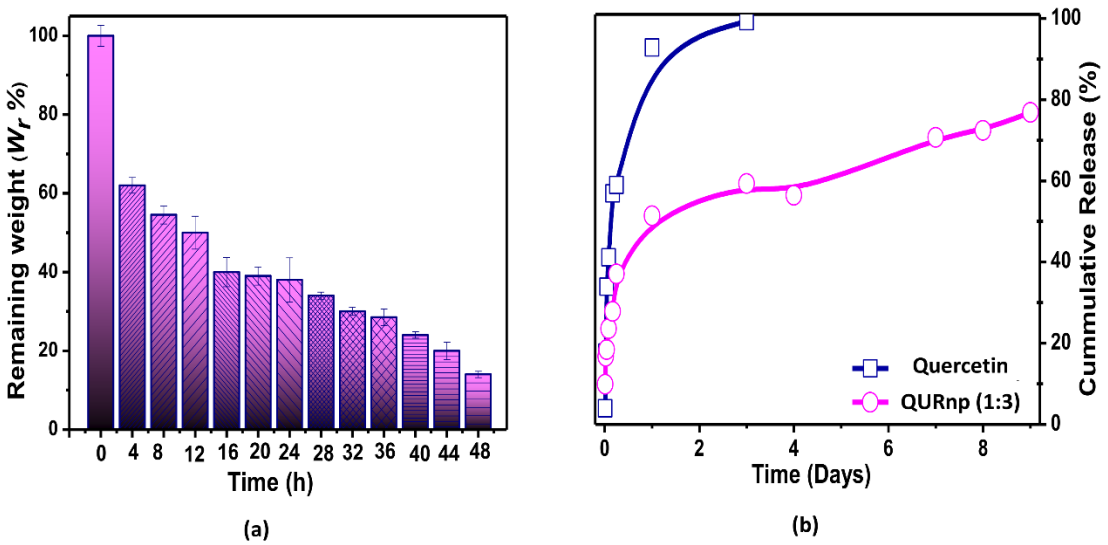

Figure 3. (a) *In-vitro* enzymatic degradation patterns of pluronic F-108; **(b)** the release study of the quercetin-loaded pluronic F-108 nanoparticles (QURnp). The degradation and release studies were carried out at 37°C in PBS, pH 7.4, and the values are an average of three triplicates.

3.3. Antitumor activity of QUR and QURnp in EAC model.

In Figure 4, vehicle 1&2 displayed no significant change in tumor volume compared to the EAC group. Treatment of free QUR at a dose of 10 mg/kg revealed a highly significant ($p<0.01$) reduction in tumor volume and a significant ($p<0.05$) reduction in viability, but at doses of 25 and 50 mg/kg displayed an extremely significant ($p<0.001$) decrease in tumor volume and also exhibited a highly significant ($p<0.01$) and extremely significant ($p<0.001$) decrease respectively in viability compared to EAC control group. Additionally, QURnp at doses 10 and 25mg/kg demonstrated an extremely significant ($p<0.001$) decrease in tumor volume and viability compared to the control group. At the same time, treatment of QURnp at a high dose of 50mg/kg demonstrated destruction of EAC cells, which resulted from the disappearance of ascetic fluid.

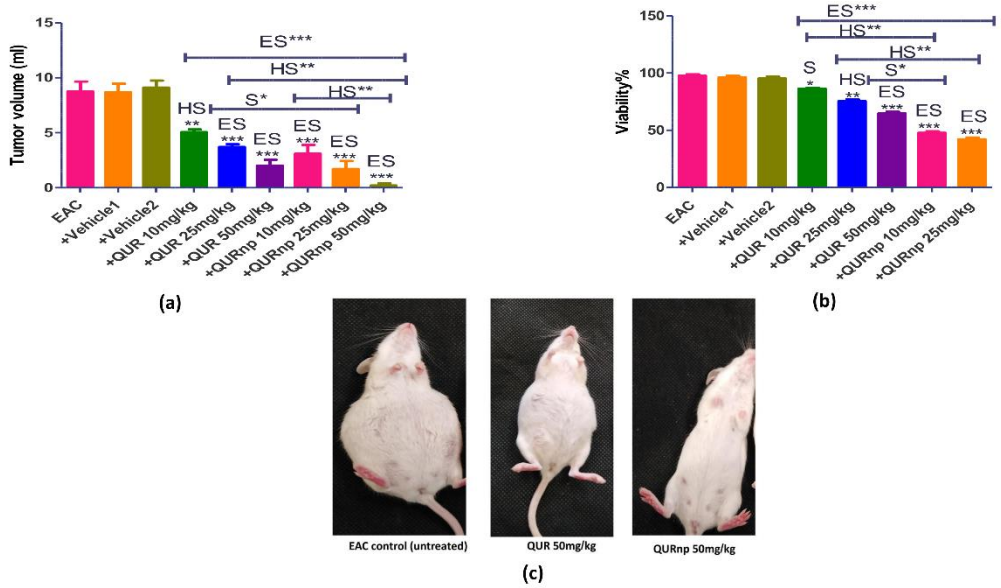

Figure 4. Antitumor effect of QUR and its nanoformulation **(a)**Tumor volume (ml) ; **(b)**Viability percentage (%) in mice treated with different doses of Quercetin (QUR) (10, 25, and 50 mg/kg) and Quercetin -loaded Pluronic nanoparticles (QURnp) (10, 25 and 50 mg/kg)) compared to EAC control group (mean±SE). **(c)** Effect

of QUR and QURnp at a dose of (50 mg/kg) on EAC-bearing mice, QURnp showed complete destruction of tumor cells. Significant (S* <0.05), Highly Significant (HS**<0.01) and Extremely Significant (ES***<0.001)

3.4. Antioxidant activity of QUR and QURnp in tumor cells.

GSH is a crucial intracellular antioxidant that regulates the cellular redox state and protects the cells from injury induced by free radicals. Figure 5a showed that treatment of free QUR at a dose of 10 mg/kg didn't show a significant effect on GSH levels in tumor cells, but at doses of 25 and 50mg/kg displayed a highly significant ($p<0.01$) and extremely significant ($p<0.001$) increase respectively compared to EAC control group. Treatment with QURnp at both doses of 10 and 25mg/kg displayed an extremely significant ($p<0.001$) increase in GSH content in EAC cells. Our results demonstrated that QUR nanoformulation at the dose of 25mg/kg induced the potential impact on GSH level in tumor cells compared to free QUR.

Furthermore, SOD and CAT are considered the first-line defense antioxidant, which is essential in the entire defense mechanism of antioxidants [41]. As shown in (Figure 5b,c), both doses 10 and 25mg/kg of free QUR exhibited significant ($p<0.05$) and highly significant ($p<0.01$) elevation, respectively, in the activity of SOD and CAT in EAC cells, as compared to the control group, while a dose of 50mg/kg, demonstrated an extremely significant ($p<0.001$). In addition, QURnp administration at doses of 10 and 25mg/kg exhibited an extremely significant ($p<0.001$) elevation in SOD and CAT activity compared to the control group, which reveals the superiority of QURnp treatment over its native QUR.

Finally, QURnp at the dose of 25mg/kg showed a very significant restoration in the activity of the antioxidant enzymes of SOD and CAT.

On the other hand, high rates of reactive oxygen species (ROS) have been noticed in cancer types, where they give multiple aspects of tumor growth and progression [42].

In Figure 5d, the treatment of native QUR at doses of 10 and 25 mg/kg displayed a highly significant ($p<0.01$) decrease in MDA level as a lipid peroxidation biomarker when compared to EAC group and high dose of native QUR 50mg/kg displayed extremely significant ($p<0.001$) reduction in MDA levels. Furthermore, MDA levels were extremely significant ($p<0.001$) decreased in QURnp at doses of 10, and 25mg/kg treated groups.

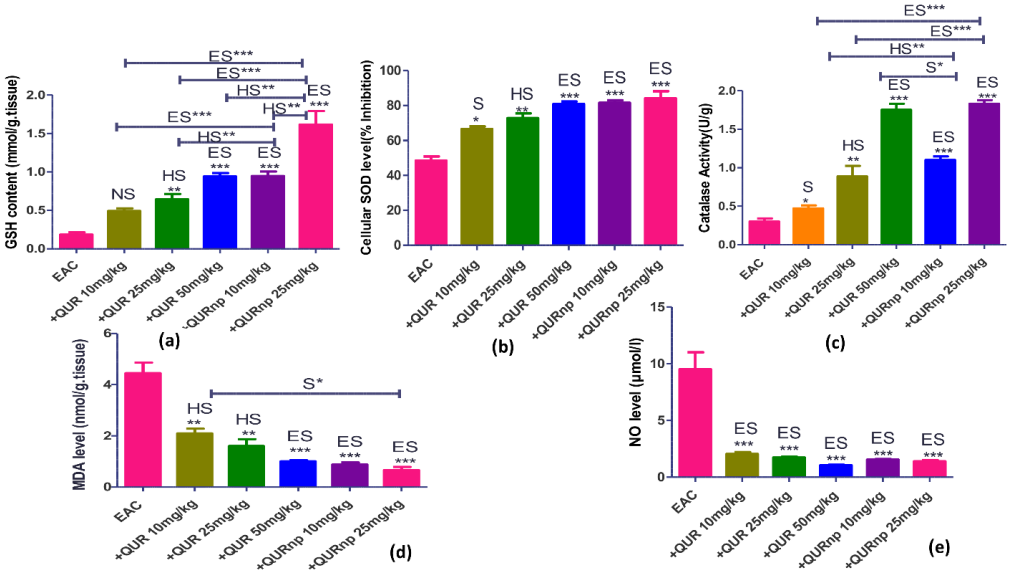

Figure 5. Antioxidant activity QUR and QURnp. **(a)** GSH content (mmol/g.tissue); **(b)** Cellular SOD level (% Inhibition); **(c)** Catalase activity (U/g); **(d)** MDA level (nmol/g.tissue); **(e)** NO level (µmol/l) in (QUR) (10, 25 and 50 mg/kg) and (QURnp) (10 and 25 mg/kg) compared to EAC-bearing mice control group (mean±SE).

Non-Significant (NS), Significant (S* <0.05), Highly Significant (HS**<0.01), and Extremely Significant (ES***<0.001).

Additionally, in Figure 5e, the administration of native QUR and its nanoformulation at different doses of 10 and 25 mg/kg revealed an extremely significant ($p<0.001$) decrease in NO levels compared to the EAC control group.

3.5. Effect of QUR and QURnp on Hematological Parameters.

In Table S2, the values of WBC were found to decrease along with an increase in the RBC count and hemoglobin content in both native QUR and QURnp-treated groups at different doses compared to the EAC control group. Furthermore, it is worth mentioning that none of the treated mice with different doses of QURnp didn't exhibit any unfavorable signs, revealing that QURnp is safe and effective in cancer therapy.

3.6. Histopathological results.

Light microscopic investigation of the EAC inoculated group displayed massive tumor growth with a notable level of cellular pleomorphism along with an increased number of mitotic figures and a remarkable loss of characteristic cellular features. Also, the EAC group was characterized by eosinophilic cytoplasm and basophilic nuclei. (10mg/kg) QUR-treated groups exhibited almost the same profiles as the former group pointing out that this dose is too small to exert an effect on EAC inoculated group. On the other hand, (25, 50mg/kg) QUR-treated animals and (10, 25 mg/kg) QURnp showed mild to huge damage to EAC cells in a dose-dependent manner when compared to the EAC group. Moreover, (50mg/kg) QURnp drug presents an immense destructive influence on EAC-treated cells to the point of the impossibility of collecting any ascites cells referring to the powerful impact of that QURnp dose. Moreover, QURnp exhibited preponderance over native drugs of the same doses, as shown in Figure 6.

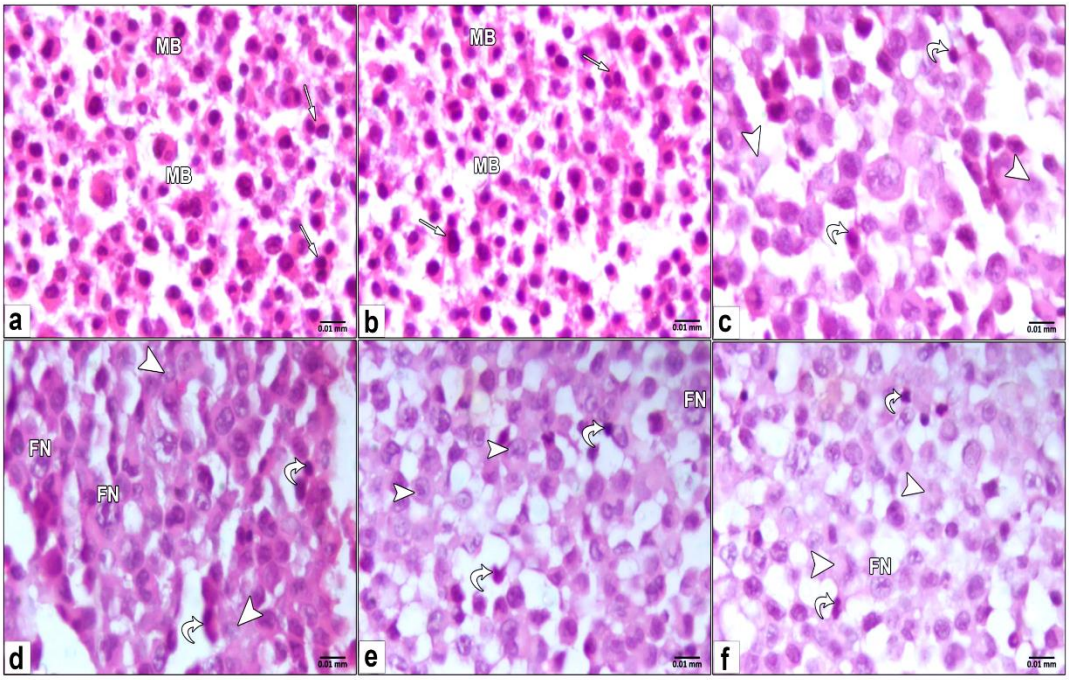

Figure 6. EAC cells sections of (**a)** control mice showing standard Ehrlich cells with membrane blebs (MB) and mitotic figures (white arrows); (**b)** QUR (10mg/kg) dose showing alike the control group; **(c)** QUR (25mg/kg); **(d)** QUR (50mg/kg) ; **(e) (**10mg/kg) of QURnp showing progressive destruction in EAC cells compared to

control group; (**f)** (25mg/kg) QURnp displayed the utmost destructive signs (arrowhead) apoptotic cells, (curved arrow) pyknotic cells (FN) fragmented nucleus, (H&E stain).

Liver samples of EAC and 10 mg/kg dose of QUR-treated animals displayed notable injuries within hepatocytes illustrated in the accumulation of EAC cells and lymphocytic infiltration. Besides, there was clear sinusoidal widening in addition to activated Kupffer cells. In contrast to the previous two groups, (25, 50 mg/kg) of native QUR and (10, 25, 50 mg/kg) of QURnp displayed marked recovery for most of the hepatic structure corresponding to dose when compared to the positive control group. It is noteworthy that QURnp of the same doses excelled over the rest of the native drug-treated groups. Interestingly, (50mg/kg) QURnp exhibited top betterment of hepatic architectures compared to the rest of the treated groups indicating the perfection of this nano dose as shown in Figure 7.

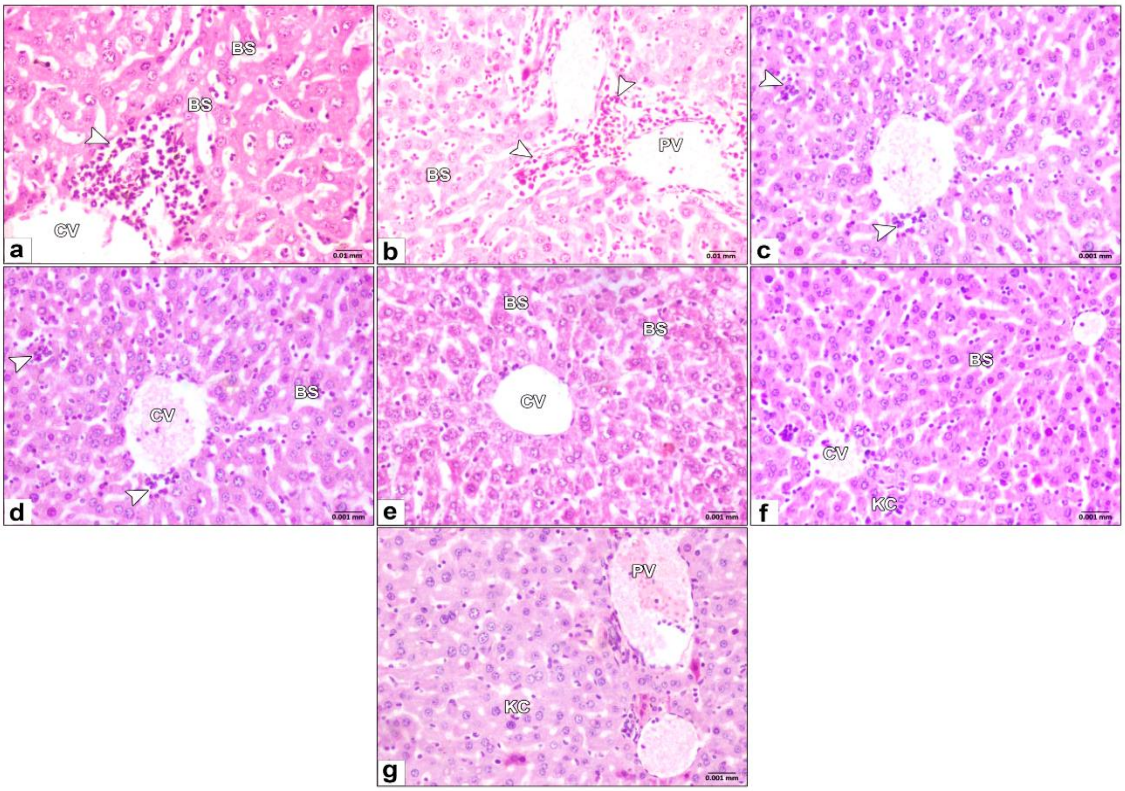

Figure 7. Liver sections of **(a)** EAC inoculated mice; (**b)** (10mg/kg) QUR treated mice displaying massive accumulation of EAC cells around the central vein (CV), dilated blood sinusoids (BS), activated Kupffer cells (KC); **(c)** (25mg/kg) QUR; **(d)** (50mg/kg) QUR treated mice showed gradual recovery of the hepatic structure proportional to dose; **(e)** (10mg/kg) QURnp; **(f) (**25mg/kg) QURnp; **(g)** (50mg/kg) QURnp treated mice exhibited progressive restoration of the liver structure in a dose-dependent manner, (H&E stain).

Kidney specimens of the EAC inoculated group and the 10mg/kg QUR treated group displayed clear injuries between glomeruli and capsules widened, glomeruli shrinkage, and the presence of some ascetic cells' infiltration. Opposite to the previously mentioned groups, the remaining treated groups displayed progressive restoration of most renal traits. 50mg/kg QURnp treated group strikingly showed the ultimate improvement compared to the remaining groups indicating the excellence of this QURnp dose. Remarkably, QURnp with different doses displayed more amelioration in EAC inoculated groups than that treated with the native drug of the same doses as in Figure 8.

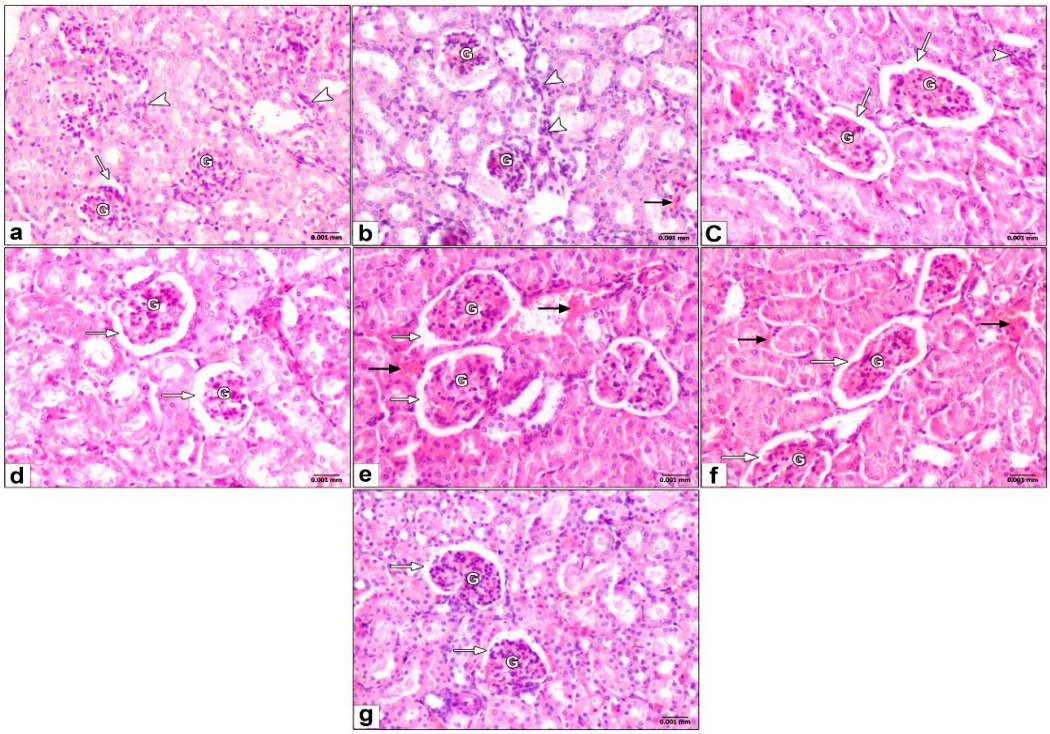

Figure 8. Kidney sections of **(a)** EAC inoculated mice**; (b)** (10mg/kg) QUR treated mice showing notable shrinkage in glomerular mass (G), spaces between renal capsule and glomerulus (white arrow) showing marked dilatation, aggregated tumor cells (arrowheads), congested renal areas (black arrow); **(c)** (25mg/kg) QUR; **(d)** (50mg/kg) QUR respectively treated groups displaying ascending improvement in renal structures; **(e)** (10 mg/kg) QURnp; **(f)** (25 mg/kg) QURnp; (**g)** (50 mg/kg) QURnp doses respectively treated groups showing palpable amelioration in kidney structure towards the typical one, (H&E stain).

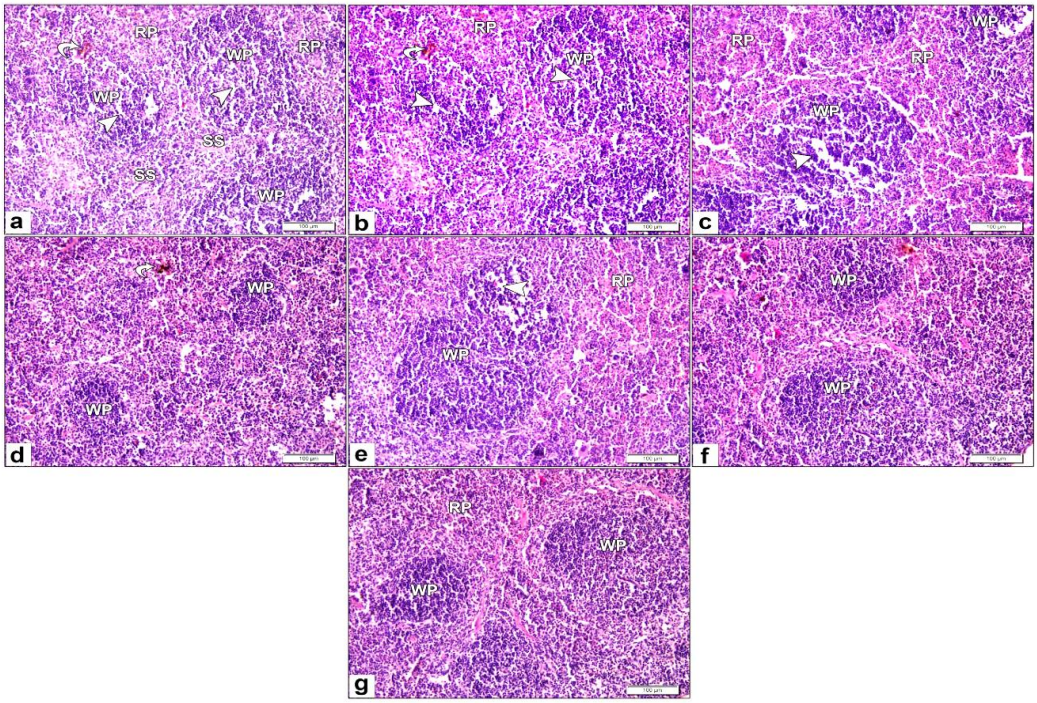

Figure 9. Spleen sections of **(a)** EAC inoculated mice; **(b)** (10mg/kg) QUR treated mice exhibiting decreased cellularity of white pulp (WP), red pulp (RP), hemosiderosis (curved arrow), congested dilated splenic sinusoids (SS); **(c)** (25 mg/kg) QUR; **(d)** (50 mg/kg) QUR respectively treated groups showing remarkable amelioration in splenic architecture; **(e)** (10 mg/kg) QURnp; **(f)** (25 mg/kg) QURnp; **(g)** (50 mg/kg) QURnp doses respectively treated animals showing clear restoration of splenic structures, (H&E stain).

The collected spleen of EAC-inoculated animals exhibited less cellularity among white pulp zones. Dilated and congested blood sinusoids within red pulp zones were also located. Similarly, 10mg/kg QUR-treated animals displayed the same results. In contrast to the former groups, the rest of the treated animals showed notable recovery for the spleen in a dose-dependent manner. It's noteworthy that QURnp-treated animals showed great amelioration with that treated with the innate one. Moreover, the spleen of 50mg/kg QURnp treated animals exhibited the perfect improvement of splenic features compared with the rest of the groups indicating the powerful curative influence of such a dose, as shown in Figure 9.

3.7. Ultrastructural results.

Electron microscope examination of the EAC group displayed typical features of cancer cells illustrated in; nonuniformed cells with asymmetrical surfaces provided with membrane blebs-like projections. Moreover, healthy mitochondrial surrounded the nuclei with prominent cristae. Similar features were displayed by 10 mg/kg QUR-treated animals, referring to an ineffectual dose for treatment. Contrariwise, other treated groups presented noticeable damage among innate QUR or QURnp-treated EAC inoculated animals. These destructive profiles are illustrated in cell shrinkage, absence of membrane blebs, pyknotic nuclei with condensed chromatin, swallowed cell membrane, and atrophied mitochondria with diminished membrane and loss of their cristae. All previously stated destructive signs were proportional to the dose and type of prepared treatment, as QURnp exhibited superiority of devastation compared with native QUR.

Moreover, the QURnp drug offered better results than the native one, directly proportional to the dose. Amazingly, 25 mg/kg of QURnp revealed the greatest damaging marks compared to the other investigated groups. We failed to collect any ascitic fluid for 50 mg/kg of QURnp-treated animals, indicating a considerable potential of that nano dose of QUR in combating EAC cells, as shown in Figure 10.

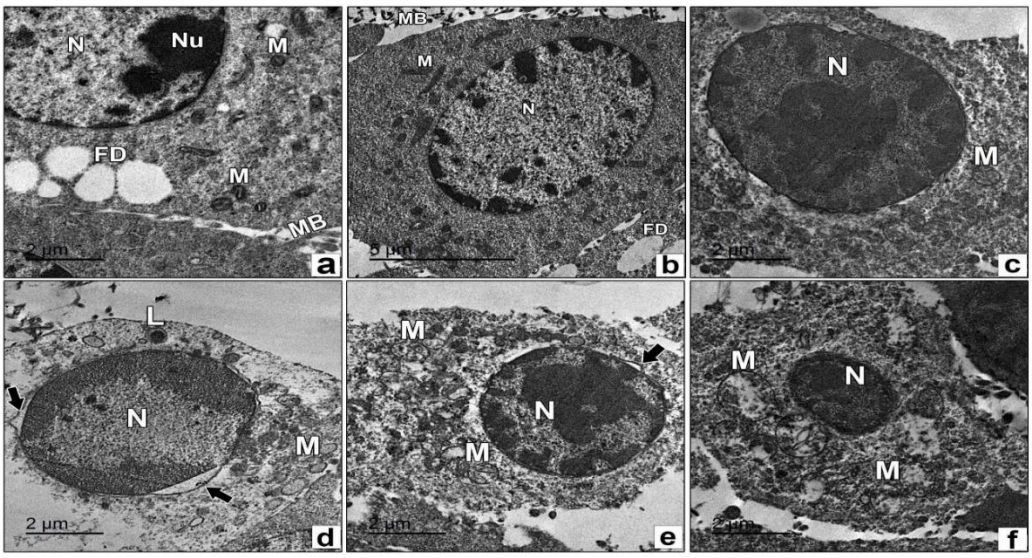

Figure 10. Transmission electron micrograph of Ehrlich ascites carcinoma cells of **(a)** control mice; **(b)** (10mg/kg) QUR treated mice showing the standard, irregular shape of tumor cells with round to oval shaped nucleus (N), nucleolus (Nu), membrane blebs (MB) surrounding cells, evident mitochondria (M); **(c)** (25 mg/kg) QUR; **(d)** (50 mg/kg) QUR respectively treated groups showing swollen nuclear membrane (black arrow), fat droplets (FD); **(e)** (10 mg/kg) QURnp; **(f)** (25 mg/kg) QURnp doses respectively treated mice displaying massive destruction of Ehrlich cells including atrophy of mitochondrial profiles, the occurrence of the lysosome (L), and apoptotic bodies.

3.8. QUR and QURnp induce cell cycle arrest and inhibit the IL-6/STAT3 pathway.

The results in Figure 11a showed that native QUR and its nanoformulation at different doses exhibited statistically significant cell cycle arrest at the G1 phase compared to the EAC control group. The greatest effect was induced by treatment with QURnp compared to its native.

Furthermore, as quercetin and its nanoformulation caused G1arrest in EAC cells so, we performed western blotting to examine the expression of p27, which is associated with G1 cell cycle arrest. As illustrated in Figure 11b, treatment of QURnp at doses of 10 and 25 mg/kg showed an increase in p27 protein levels. The present results indicate the superiority of QURnp over its native QUR-treated group.

Quercetin is able to affect various signaling pathways, for example, the STAT3 pathway. The results shown in Figure 11b demonstrated that administration of QUR and QURnp in a dose-dependent manner reduced the expression of STAT3 and p-STAT3, and QURnp can inhibit the activation of the STAT3 pathway effectively due to the decreased p-STAT3 activation.

We performed an ELISA assay to estimate IL-6 level and RT-PCR for VEGF expression to confirm the suppression of the STAT3 signaling pathway. In Figure 11c, the EAC group stimulated the release of IL-6. In contrast, both QUR and QURnp treatment at different doses of EAC-bearing mice exhibited significant ($p<0.01$), ($p<0.001$) suppression releasing of cytokine IL-6, which induced activation of STAT3.

As shown in Figure 11d, the administration of native QUR at different doses led to a significant downregulation in VEGF gene expression compared to the EAC group. Also, QURnp treated group showed extremely significant downregulation in VEGF gene expressions ($p < 0.001$) as a result of inhibition of STAT3 signaling when compared with the free QUR-treated group.

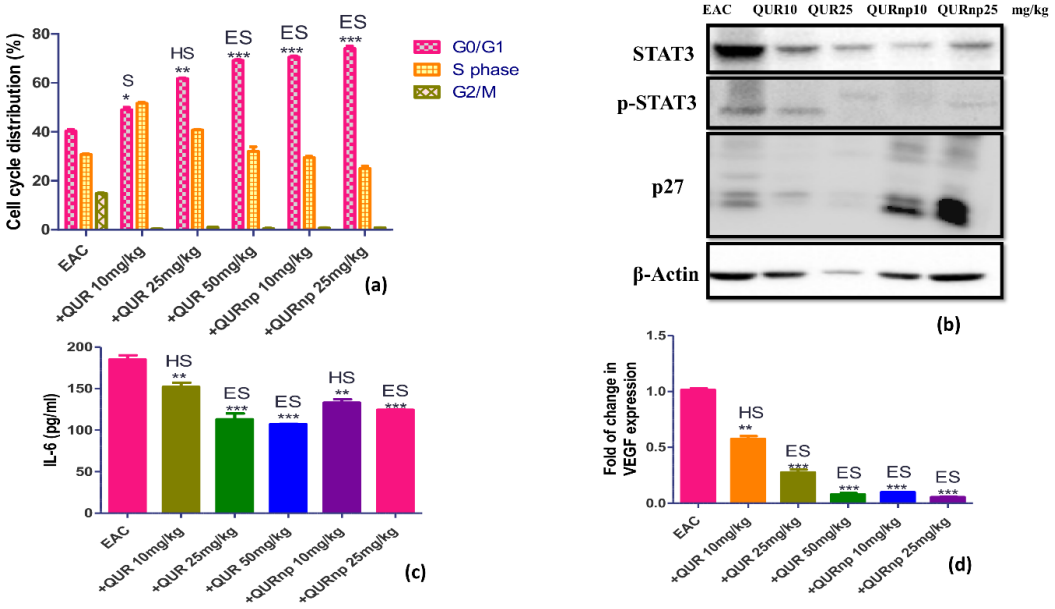

Figure 11. Anticancer mechanism of QUR and QURnp **(a)** Cell cycle progression assays were performed on EAC cells treated with different doses of QUR and QURnp; (**b)** Western blotting of p27, STAT3, and p-STAT3 in EAC cells treated with QUR and QURnp; **(c)** IL-6 level in EAC cells treated with different doses of QUR and QURnp compared to EAC control group (mean±SE); **(d)** Quantitative real-time RT-PCR (qRT-PCR) analysis of angiogenesis-related gene (VEGF) in EAC cells treated with QUR and QURnp.
Significant (S* <0.05), Highly Significant (HS**<0.01), and Extremely Significant (ES***<0.001).

3.9. Immunohistochemical results.

Ki-67 immunohistochemical investigations displayed high EAC scores and 10 mg/kg QUR treated groups too. However, the remaining groups revealed a meaningful drop in the score compared to the control group. Furthermore, QURnp-treated animals exhibited a significant fall in score compared to innate drugs with less proliferation. As expected from the previous results, 25 mg/kg of QURnp also displayed the lowest score, indicating a lesser proliferation level among all investigated groups, as shown in Figure 12.

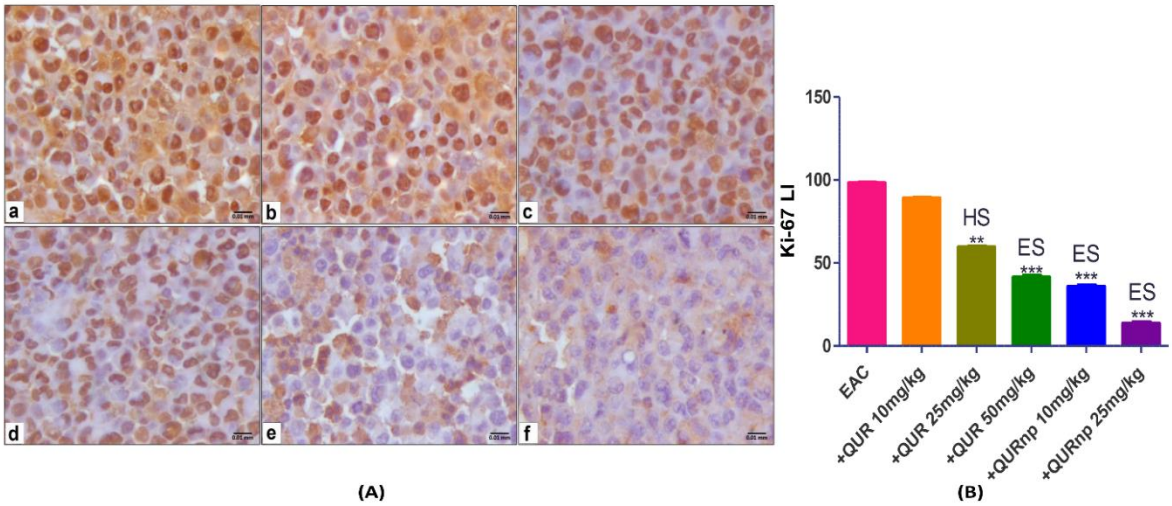

Figure 12. (A) Immunohistochemical studies of EAC cells sections of **(a)** control mice; **(b)** (10mg/kg) QUR displaying high nuclear expression of Ki-67; **(c)** (25 mg/kg) QUR; **(d)** (50 mg/kg) QUR; **(e)** (10mg/kg) QURnp respectively treated mice displaying mild expression; **(f)** (25 mg/kg) QURnp displayed weak nuclear expression, (IHC); **(B)** Labeling index chart of Ki-67 among investigated groups.
Highly Significant (HS**<0.01) and Extremely Significant (ES***<0.001).

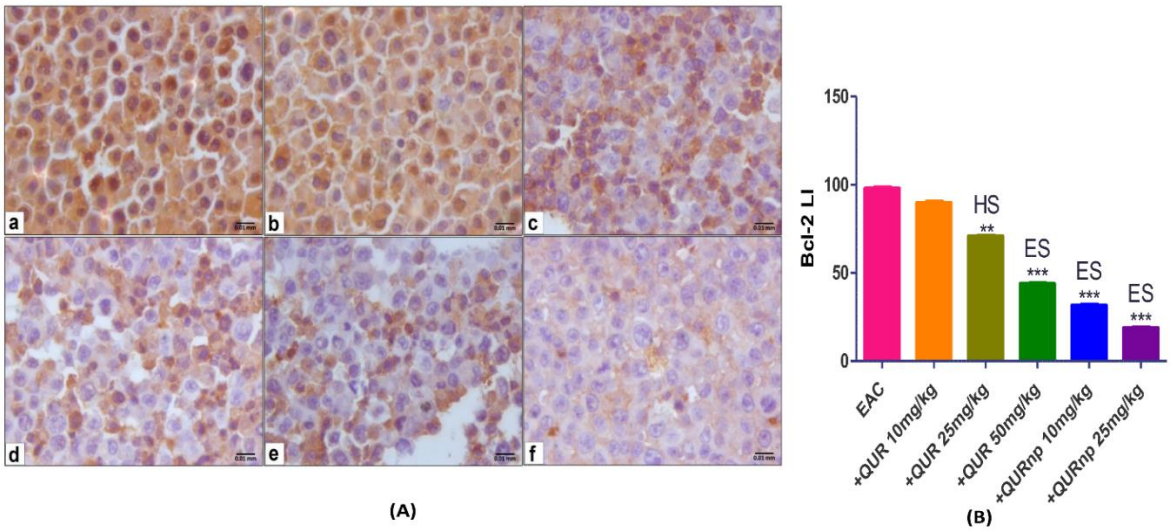

Figure 13. (A) Immunohistochemical studies of EAC cells sections of **(a)** control mice; **(b)** (10mg/kg) QUR displaying a high cytoplasmic expression of Bcl-2; **(c)** (25 mg/kg) QUR; **(d)** (50 mg/kg) QUR; **(e)** (10mg/kg) QURnp respectively treated mice displaying mild expression; **(f)** (25 mg/kg) QURnp displayed weak cytoplasmic expression, (IHC). **(B)** Labeling index chart of Bcl-2 among investigated groups.
Highly Significant (HS**<0.01) and Extremely Significant (ES***<0.001).

Bcl-2 labeling index displayed an almost similar high score in the case of the control group and 10 mg/kg of QUR-treated groups as well. Whereas (20, 50 mg/kg) of QUR and (10, 25 mg/kg) of QURnp as a well displayed significant drop of score in a dose-dependent manner, denoting the marvelous action of this drug, especially 25 mg/kg of QURnp one which elucidate

the lesser score within all investigated groups and when compared to control one as displayed in Figure 13.

4. Discussion

Recently, combining phytochemicals with nanotechnology can be a vital tool for advancing phytochemicals as cancer therapeutic agents with enhanced bioavailability and solubility [43]. Thus, the present study aimed to fabricate a stable nanoformulation of QUR and demonstrate its potential in cancer treatment using mice-bearing EAC cells as a cancer model. Our results showed promising chemotherapeutic anticancer properties of QURnp by destroying of tumor at a dose of 50 mg/kg. QURnp can lead to a more significant decrease in tumor growth and cell viability than native QUR at the same dose. Furthermore, our present investigations agree with recent reports, which stated that quercetin nanoparticles are more effective than native QUR in cancer treatment via inhibition of proliferation and tumor growth [17,44-46]. El-Far *et al*. showed the superiority of pluronic nanoparticles in drug delivery because of their novel properties to improve solubility, bioavailability, and prolonged drug release; they also demonstrated that phytochemicals (Silymarin and Curcumin) loaded pluronic nanoparticles have great potential to suppress the growth of tumor than their native in EAC-bearing mice [19,20]. So, these advantages enable QURnp to be superior in cancer therapy.

QUR has potent antioxidant effects and promising activity against oxidative damage, which acts as ROS scavengers and inhibits ROS activity. The antioxidant activity of QUR is mainly manifested through its effect on glutathione (GSH) and enzymatic activity such as (SOD, CAT). In the present results, the EAC-bearing mice group demonstrated a significant decrease in SOD, CAT, and GSH levels when compared to treated groups which is in accordance with others [47]. GSH has a significant role in antioxidant defenses via detoxifying free radicals. So, QUR and QURnp showed an increase in cellular GSH levels. It has been reported that QUR can regulate GSH levels and induce the synthesis of GSH [48]. QURnp (25 mg/kg) showed the highest significant increase in GSH level compared to the control group and native QUR-treated groups (25 mg/kg & 50 mg/kg).

Furthermore, SOD and CAT constitute a crucial antioxidant defense against reactive oxygen species-mediated diseases in the body. According to the present data, we herein indicated a significant elevation in SOD and CAT activity in both QUR and QURnp-treated groups when compared to the EAC control group. At the same time, treatment with QURnp at a dose (25 mg/kg) exhibited a more pronounced significant increase in SOD and CAT activity. It has been found that SOD levels markedly increased in QUR-loaded polymeric nanoparticles-treated tumor-bearing mice than free QUR-treated group, which is in agreement with our present findings [17]. On the other hand, QUR fights cancer by modulating oxidative stress markers such as lipid peroxidation (LPO) and reactive nitrogen species (RNS) [49], which in turn led to a statistically significant reduction in MDA and NO levels in treated groups with QUR and QURnp in a dose-dependent manner. Consistent with our findings, other investigators reported that QUR nanoformulation increased antioxidant biomarkers (SOD, CAT, and GSH) and attenuated lipid peroxidation [50]. This is mainly due to the improvement of QUR solubility and bioavailability. Finally, our data strongly indicate that QURnp is a superior antioxidant and anticancer agent over native QUR.

In our study, the EAC control group showed a decrease in hemoglobin, RBC count and an increased WBC count due to myelopathic or hemolytic conditions. In contrast, the administration of QUR and QURnp can replenish the Hb content and maintain the normal RBC

and WBC values. This indicates that QURnp treatment possesses a protective effect on the hematopoietic system. QUR is a well-known antioxidant with anti-inflammatory properties [51], which may be the reason for its hematopoietic activity.

EAC cells are known for their immense transplantable average, rapid proliferation, and limited survival duration can cause complete mortality and hyperdiploid [52,53]. Thus, EAC was assigned in this study to investigate the potential impact of QUR on it, whether in its native or QURnp. Our histopathological findings showed the considerable effect of QUR on eliminating EAC cells, which was in consonance with Yılmaz *et al*. [54].

Liver samples of the EAC control group exhibited massive damage; scattered necrotic foci, extended blood sinusoids, activated Kupffer cells, and congested blood vessels with notable lymphocytic infiltration. Abd Eldaim and Tousson also confirmed the previous outcomes [55,56]. On the other hand, high doses of QUR, in addition to QURnp ones, displayed marked restoration of most of the hepatic architecture lost by EAC cells. Remarkably, 50 mg/kg of QURnp displayed the most ameliorative signs within the hepatic structure.

Kidney specimens of EAC inoculated animals showed notable degenerated renal marks like; atrophied glomeruli, expanded space between glomerulus and its capsule, and degenerated renal tubules. These results match those of Medhat, who suggested EAC's likely action, which activates ROS generation that devastates cellular homeostasis and consequently leads to damaged tissue [57]. In contrast, the remaining QUR-treated groups displayed remarkable recovery in a dose-dependent manner. According to Sanchez-Gonzalez *et al*., the main influence of QUR on renal damage is to lessen inflammation and oxidative stress and to stabilize the renal blood flow [58]. Min and Ebeler *et al*. stated that a high concentration of QUR displayed an evident antitumor effect via binding to neoplastic cells' DNA [59]. Our results highlighted the distinction of QURnp over the native QUR of the same dose.

Spleen samples of positive control and/or 10 mg/kg QUR groups displayed various degenerations, such as decreased cellularity in the white pulp, widened congested blood sinusoids, and some focal deposits of hemosiderin surrounding hemorrhage sites. Based on animal research, QUR accumulates at low doses in the spleen that is disposed of through the respiratory, fecal, and renal systems [60,61]. Nevertheless, the spleen of animals treated with higher doses of QUR in addition to QURnp ones displayed a marked recovery compared to the previous two groups. According to Farag *et al.*, QUR has a genoprotective impact to the extent that it ameliorates depleted white pulp and lymphopenia in the spleen of Doxorubicin-treated rodents [62].

Ultrastructural findings of the control group of EAC showed typical features of cancer, and this matches with Batista *et al*. [54,63]. It is familiar that EAC cells, once inoculated intraperitoneally, divide quickly, increasing the amount of ascetic fluid proportion to the proliferation development. This fluid is considered the nutritional base for those tumor tumors cells [64]. On the other hand, QUR and QURnp exhibited noted devastation for Ehrlich cells illustrated in apoptotic cells, degenerated mitochondria, condensed nucleus, and lysosomal presence. Programmed cell death can be distinguished through certain incidents like membrane projections called membrane blebs, DNA fragmentation, and extension of cytoplasm [65-67]. It is well proven that QUR uses a mitochondrial-mediated mechanism in order to initiate its apoptotic effect [68-70]. Also, Min and Ebeler stated that QUR at high concentrations exhibits antitumor action by making a covalent bond with the DNA of cancer cells and consequently destroying it [59]. Mitochondria, which are the cell's power stations, also were affected by QUR and QURnp. Overall, a myriad of the research reported the role of QUR in inducing

mitochondrial dysfunction within neoplastic cells and its pro-apoptotic action [71]. Amazingly, QURnp-treated animals revealed noticeable damage for cancer cells, especially 50 mg/kg dose, to the extent that we couldn't collect any ascetic fluid from this group. Our study can be considered the first to evaluate the effect of QUR and its nanoformulation (QURnp) ultrastructurally.

Cell cycle dysregulation is a hallmark of cancer cells, increasing cellular proliferation. QUR can induce cell cycle arrest in many cancer cells via its effect on several target proteins, such as p27 [72]. Our data revealed that QURnp treatment in a dose-dependent manner induced cell cycle arrest at the G1/S phase via up-regulation of p27 expression and finally blocked the progression of tumor cells and decreased the EAC's proliferation rate cells. The present results agree with the previous study, which reported that QUR nanoparticles showed antitumor activity via upregulation of p27 in cancer cells which induces cell cycle arrest [73].

Previous studies have investigated the effect of QUR on the STAT3 pathway [12,74,75]. In the present study, we have demonstrated that QURnp can suppress tumor growth and invasion through the inhibition IL-6/STAT3 signaling pathway. Nanoformulation of QUR (QURnp) caused a downregulation of IL-6, inhibiting p-STAT3 expression and thus inhibiting the activation of STAT3 signaling.

Furthermore, our results suggest that the downregulation of angiogenesis accompanies the inhibition of the STAT3 pathway. Administration of QURnp showed highly effect on inhibiting the expression of VEGF, a potent angiogenic factor. Therefore QURnp exerted antitumor activity via its antiangiogenetic effect on EAC tumor cells. QUR has previously been reported to suppress *angiogenesis* in various cancer cells [76,77], but nanoformulation can enhance the anticancer efficacy of QUR, making it a potent anticancer agent over its native.

Immunohistochemical findings displayed that QUR and/or QURnp one lower Ki-67 (proliferation marker) and Bcl-2 (anti-apoptotic marker) counts among treated groups in a dose-dependent manner. In contrast, the positive control group and 10 mg/kg QUR dose recorded the highest score of both antigens. Surprisingly, the QURnp dose of 25 mg/kg reported the lowest score compared to the rest of the treated groups within both markers. Liu *et al*. explained the outstanding potential of QUR to overcome prostate cancer by lowering Bcl2 levels and stimulating caspases through the endoplasmic reticulum and mitochondrial stress [78]. According to Banerjee *et al*. and Granado-Serrano *et al*., apoptosis can be stimulated by several cellular signaling protein modifications; one of them is the downregulation of Bcl-2 [79-81].

Finally, the results suggested that QURnp is superior to its native as a chemotherapeutic anticancer agent, and also, QURnp can inhibit cancer progression via several pathways as demonstrated, indicating its effectiveness against cancer.

5. Conclusions

In the present study, our findings suggest that quercetin nanoformulation (QURnp) treatment significantly inhibits tumor growth in EAC-bearing mice via inhibiting the IL-6/STAT3 signaling pathway. In addition, administration of QURnp markedly induces cell cycle arrest and apoptosis through significantly increasing p27 as well as reduced Bcl-2 expression. QURnp exhibited a potential antioxidant role in increased SOD, CAT, and GSH levels and reduced MDA and NO levels. Furthermore, this study also shows that QURnp is a potent suppressor of angiogenesis that inhibits VEGF gene expression. Finally, QUR-loaded pluronic nanoparticles could be used as a promising drug candidate in cancer treatment.

Funding

This research received no external funding.

Acknowledgment

Professor Mohamed El-Far would like to thank Genome and Cancer Research, Urology and Nephrology Centre, Mansoura University, Mansoura, Egypt, for providing the Bio-Rad Imaging facility, and Electron Microscopy Unit, Mansoura University.

Conflicts of Interest

The authors declare no conflict of interest.

References

1. Lichota, A.; Gwozdzinski, K. Anticancer activity of natural compounds from plant and marine environment. *International journal of molecular sciences* **2018**, *19*, 3533, http://dx.doi.org/10.3390/ijms19113533.
2. Choudhari, A.S.; Mandave, P.C.; Deshpande, M.; Ranjekar, P.; Prakash, O. Phytochemicals in cancer treatment: From preclinical studies to clinical practice. *Frontiers in pharmacology* **2020**, *10*, 1614, http://dx.doi.org/10.3389/fphar.2019.01614.
3. Kopustinskiene, D.M.; Jakstas, V.; Savickas, A.; Bernatoniene, J. Flavonoids as anticancer agents. *Nutrients* **2020**, *12*, 457, http://dx.doi.org/10.3390/nu12020457.
4. Thomasset, S.C.; Berry, D.P.; Garcea, G.; Marczylo, T.; Steward, W.P.; Gescher, A.J. Dietary polyphenolic phytochemicals—promising cancer chemopreventive agents in humans? A review of their clinical properties. *International journal of cancer* **2007**, *120*, 451-458, http://dx.doi.org/10.1002/ijc.22419.
5. Azeem, M.; Hanif, M.; Mahmood, K.; Ameer, N.; Chughtai, F.R.S.; Abid, U. An insight into anticancer, antioxidant, antimicrobial, antidiabetic and anti-inflammatory effects of quercetin: A review. *Polymer Bulletin* **2022**, 1-22, http://dx.doi.org/10.1007/s00289-022-04091-8.
6. Srivastava, S.; Somasagara, R.R.; Hegde, M.; Nishana, M.; Tadi, S.K.; Srivastava, M.; Choudhary, B.; Raghavan, S.C. Quercetin, a Natural Flavonoid Interacts with DNA, Arrests Cell Cycle and Causes Tumor Regression by Activating Mitochondrial Pathway of Apoptosis. *Sci Rep* **2016**, *6*, 24049, http://dx.doi.org/10.1038/srep24049.
7. Shafabakhsh, R.; Asemi, Z. Quercetin: a natural compound for ovarian cancer treatment. *J Ovarian Res* **2019**, *12*, 55, http://dx.doi.org/10.1186/s13048-019-0530-4.
8. Mirazimi, S.M.A.; Dashti, F.; Tobeiha, M.; Shahini, A.; Jafari, R.; Khoddami, M.; Sheida, A.H.; EsnaAshari, P.; Aflatoonian, A.H.; Elikaii, F. Application of Quercetin in the Treatment of Gastrointestinal Cancers. *Frontiers in Pharmacology* **2022**, *13*, http://dx.doi.org/10.3389/fphar.2022.8602.
9. Chen, B.; Wu, L.; Tang, X.; Wang, T.; Wang, S.; Yu, H.; Wan, G.; Xie, M.; Zhang, R.; Xiao, H. Quercetin Inhibits Tumorigenesis of Colorectal Cancer Through Downregulation of hsa_circ_0006990. *Frontiers in Pharmacology* **2022**, *13*, http://dx.doi.org/10.3389/fphar.2022.87469.
10. Ghafouri-Fard, S.; Shabestari, F.A.; Vaezi, S.; Abak, A.; Shoorei, H.; Karimi, A.; Taheri, M.; Basiri, A. Emerging impact of quercetin in the treatment of prostate cancer. *Biomedicine & Pharmacotherapy* **2021**, *138*, 111548, http://dx.doi.org/10.1016/j.biopha.2021.111548.
11. Tang, S.-M.; Deng, X.-T.; Zhou, J.; Li, Q.-P.; Ge, X.-X.; Miao, L. Pharmacological basis and new insights of quercetin action in respect to its anticancer effects. *Biomedicine & Pharmacotherapy* **2020**, *121*, 109604, http://dx.doi.org/10.1016/j.biopha.2019.109604.
12. Vafadar, A.; Shabaninejad, Z.; Movahedpour, A.; Fallahi, F.; Taghavipour, M.; Ghasemi, Y.; Akbari, M.; Shafiee, A.; Hajighadimi, S.; Moradizarmehri, S. Quercetin and cancer: new insights into its therapeutic effects on ovarian cancer cells. *Cell & bioscience* **2020**, *10*, 1-17, http://dx.doi.org/10.1186/s13578-020-00397-0.
13. Rasool, M.; Malik, A.; Waquar, S.; Arooj, M.; Zahid, S.; Asif, M.; Shaheen, S.; Hussain, A.; Ullah, H.; Gan, S.H. New challenges in the use of nanomedicine in cancer therapy. *Bioengineered* **2022**, *13*, 759-773, http://dx.doi.org/10.1080/21655979.2021.2012907.

14. Anwar, D.M.; El-Sayed, M.; Reda, A.; Fang, J.-Y.; Khattab, S.N.; Elzoghby, A.O. Recent advances in herbal combination nanomedicine for cancer: delivery technology and therapeutic outcomes. *Expert opinion on drug delivery* **2021**, *18*, 1609-1625, http://dx.doi.org/10.1080/17425247.2021.1955853.
15. Zang, X.; Cheng, M.; Zhang, X.; Chen, X. Quercetin nanoformulations: A promising strategy for tumor therapy. *Food & Function* **2021**. http://dx.doi.org/10.1039/D1FO00851J.
16. Men, K.; Duan, X.; Wei Wei, X.; Ling Gou, M.; Juan Huang, M.; Juan Chen, L.; Yong Qian, Z.; Quan Wei, Y. Nanoparticle-delivered quercetin for cancer therapy. *Anticancer Agents in Medicinal Chemistry (Formerly Current Medicinal Chemistry-Anti-Cancer Agents)* **2014**, *14*, 826-832, http://dx.doi.org/10.2174/1871520614666140521122932.
17. Baksi, R.; Singh, D.P.; Borse, S.P.; Rana, R.; Sharma, V.; Nivsarkar, M. *In vitro* and *in vivo* anticancer efficacy potential of quercetin loaded polymeric nanoparticles. *Biomedicine & Pharmacotherapy* **2018**, *106*, 1513-1526, http://dx.doi.org/10.1016/j.biopha.2018.07.106.
18. Vinayak, M.; Maurya, A.K. Quercetin loaded nanoparticles in targeting cancer: recent development. *Anticancer Agents in Medicinal Chemistry (Formerly Current Medicinal Chemistry-Anti-Cancer Agents)* **2019**, *19*, 1560-1576, http://dx.doi.org/10.2174/1871520619666190705150214.
19. El-Far, M.; Salah, N.; Essam, A.; Abd El-Azim, A.; Karam, M.; El-Sherbiny, I.M. Potential anticancer activity and mechanism of action of nanoformulated curcumin in experimental Ehrlich ascites carcinoma-bearing animals. *Nanomedicine (Lond)* **2019**, *14*, 553-573, http://dx.doi.org/10.2217/nnm-2018-0298.
20. El-Far, M.; Salah, N.; Essam, A.; Abd El-Azim, A.O.; El-Sherbiny, I.M. Silymarin nanoformulation as potential anticancer agent in experimental Ehrlich ascites carcinoma-bearing animals. *Nanomedicine* **2018**, *13*, 1865-1858, http://dx.doi.org/10.2217/nnm-2017-0394.
21. Tiwari, S.; Kansara, V.; Bahadur, P. Targeting anticancer drugs with pluronic aggregates: Recent updates. *International Journal of Pharmaceutics* **2020**, *586*, 119544, http://dx.doi.org/10.1016/j.ijpharm.2020.119544.
22. Yu, J.; Qiu, H.; Yin, S.; Wang, H.; Li, Y. Polymeric drug delivery system based on pluronics for cancer treatment. *Molecules* **2021**, *26*, 3610, http://dx.doi.org/10.3390/molecules26123610.
23. El-Far, Y.M.; Zakaria, M.M.; Gabr, M.M.; El Gayar, A.M.; Eissa, L.A.; El-Sherbiny, I.M. Nanoformulated natural therapeutics for management of streptozotocin-induced diabetes: potential use of curcumin nanoformulation. *Nanomedicine* **2017**, *12*, 1689-1711, http://dx.doi.org/10.2217/nnm-2017-0106.
24. El-Far, M.; Elshal, M.; Refaat, M.; El-Sherbiny, I.M. Antitumor activity and antioxidant role of a novel water-soluble carboxymethyl chitosan-based copolymer. *Drug Dev Ind Pharm* **2011**, *37*, 1481-1490, http://dx.doi.org/10.3109/03639045.2011.587430.
25. Green, L.C.; Wagner, D.A.; Glogowski, J.; Skipper, P.L.; Wishnok, J.S.; Tannenbaum, S.R. Analysis of nitrate, nitrite, and [15N]nitrate in biological fluids. *Anal Biochem* **1982**, *126*, 131-138, http://dx.doi.org/10.1016/0003-2697(82)90118-x.
26. Reynolds, E.S. The use of lead citrate at high pH as an electron-opaque stain in electron microscopy. *J Cell Biol* **1963**, *17*, 208-212, http://dx.doi.org/10.1083/jcb.17.1.208.
27. Gentile, L.B.; Queiroz-Hazarbassanov, N.; Massoco, C.d.O.; Fecchio, D. Modulation of cytokines production by indomethacin acute dose during the evolution of Ehrlich ascites tumor in Mice. *Mediators of Inflammation* **2015**, *2015*, http://dx.doi.org/10.1155/2015/924028.
28. Thirusangu, P.; Vigneshwaran, V.; Ranganatha, V.L.; Vijay Avin, B.R.; Khanum, S.A.; Mahmood, R.; Jayashree, K.; Prabhakar, B.T. A tumoural angiogenic gateway blocker, Benzophenone-1B represses the HIF-1alpha nuclear translocation and its target gene activation against neoplastic progression. *Biochem Pharmacol* **2017**, *125*, 26-40, http://dx.doi.org/10.1016/j.bcp.2016.11.009.
29. Petrosyan, K.; Tamayo, R.; Joseph, D. Sensitivity of a novel biotin-free detection reagent (Powervision+™) for immunohistochemistry. *Journal of histotechnology* **2002**, *25*, 247-250, http://dx.doi.org/10.1179/014788802794791951.
30. Chatterjee, S.; Hui, P.C.-l.; Kan, C.-w.; Wang, W. Dual-responsive (pH/temperature) Pluronic F-127 hydrogel drug delivery system for textile-based transdermal therapy. *Scientific reports* **2019**, *9*, 1-13, http://dx.doi.org/10.1038/s41598-019-48254-6.
31. Mohamed, R.; Saad, E.A.; Habib, S.A.; Waly, H.M. Loading of some quinoxaline derivatives in poly (l-lactic) acid/Pluronic® F-127 nanofibers enhances their anticancer efficiency and induces a p53 and p21 apoptotic-signaling pathway. *Colloids and Surfaces B: Biointerfaces* **2019**, *183*, 110444, http://dx.doi.org/10.1016/j.colsurfb.2019.110444.

32. Ali, I.H.; Khalil, I.A.; El-Sherbiny, I.M. Single-dose electrospun nanoparticles-in-nanofibers wound dressings with enhanced epithelialization, collagen deposition, and granulation properties. *ACS applied materials & interfaces* **2016**, *8*, 14453-14469, http://dx.doi.org/10.1021/acsami.6b04369.
33. Samarasinghe, S.A.S.C.; Chuah, C.Y.; Karahan, H.E.; Sethunga, G.; Bae, T.-H. Enhanced O2/N2 Separation of Mixed-Matrix Membrane Filled with Pluronic-Compatibilized Cobalt Phthalocyanine Particles. *Membranes* **2020**, *10*, 75. http://dx.doi.org/10.3390/membranes10040075.
34. Heggannavar, G.B.; Hiremath, C.G.; Achari, D.D.; Pangarkar, V.G.; Kariduraganavar, M.Y. Development of doxorubicin-loaded magnetic silica–pluronic F-127 nanocarriers conjugated with transferrin for treating glioblastoma across the blood–brain barrier using an *in vitro* model. *ACS omega* **2018**, *3*, 8017-8026, http://dx.doi.org/10.1021/acsomega.8b00152.
35. Bonilla-Hernández, M.; Zapata-Catzin, G.A.; Castillo-Cruz, O.d.J.; Vargas-Coronado, R.F.; Cervantes-Uc, J.M.; Xool-Tamayo, J.F.; Borges-Argaez, R.; Hernández-Baltazar, E.; Cauich-Rodríguez, J.V. Synthesis and characterization of metformin-pluronic based polyurethanes for controlled drug delivery. *International Journal of Polymeric Materials and Polymeric Biomaterials* **2021**, *70*, 656-667, http://dx.doi.org/10.1080/00914037.2020.1740996.
36. Karolewicz, B.; Gajda, M.; Pluta, J.; Górniak, A. Dissolution study and thermal analysis of fenofibrate–Pluronic F127 solid dispersions. *Journal of Thermal Analysis and Calorimetry* **2016**, *125*, 751-757, http://dx.doi.org/10.1007/s10973-015-5013-2.
37. Yang, X.; Wu, D.; Du, Z.; Li, R.; Chen, X.; Li, X. Spectroscopy study on the interaction of quercetin with collagen. *Journal of agricultural and food chemistry* **2009**, *57*, 3431-3435, http://dx.doi.org/10.1021/jf803671s.
38. Pawlikowska-Pawlęga, B.; Dziubińska, H.; Król, E.; Trębacz, K.; Jarosz-Wilkołazka, A.; Paduch, R.; Gawron, A.; Gruszecki, W.I. Characteristics of quercetin interactions with liposomal and vacuolar membranes. *Biochimica et Biophysica Acta (BBA)-Biomembranes* **2014**, *1838*, 254-265, http://dx.doi.org/10.1016/j.bbamem.2013.08.014.
39. Milanezi, F.G.; Meireles, L.M.; de Christo Scherer, M.M.; de Oliveira, J.P.; da Silva, A.R.; de Araujo, M.L.; Endringer, D.C.; Fronza, M.; Guimarães, M.C.C.; Scherer, R. Antioxidant, antimicrobial and cytotoxic activities of gold nanoparticles capped with quercetin. *Saudi pharmaceutical journal* **2019**, *27*, 968-974, http://dx.doi.org/10.1016/j.jsps.2019.07.005.
40. Alugoju, P.; Narsimulu, D.; Bhanu, J.U.; Satyanarayana, N.; Periyasamy, L. Role of quercetin and caloric restriction on the biomolecular composition of aged rat cerebral cortex: An FTIR study. *Spectrochimica Acta Part A: Molecular and Biomolecular Spectroscopy* **2019**, *220*, 117128, http://dx.doi.org/10.1016/j.saa.2019.05.033.
41. Ighodaro, O.; Akinloye, O. First line defence antioxidants-superoxide dismutase (SOD), catalase (CAT) and glutathione peroxidase (GPX): Their fundamental role in the entire antioxidant defence grid. *Alexandria journal of medicine* **2018**, *54*, 287-293, http://dx.doi.org/10.1016/j.ajme.2017.09.001.
42. Liou, G.-Y.; Storz, P. Reactive oxygen species in cancer. *Free radical research* **2010**, *44*, 479-496, http://dx.doi.org/10.3109/10715761003667554.
43. Teja, P.K.; Mithiya, J.; Kate, A.S.; Bairwa, K.; Chauthe, S.K. Herbal nanomedicines: Recent advancements, challenges, opportunities and regulatory overview. *Phytomedicine* **2021**, 153890, http://dx.doi.org/10.1016/j.phymed.2021.153890.
44. Zhou, Y.; Chen, D.; Xue, G.; Yu, S.; Yuan, C.; Huang, M.; Jiang, L. Improved therapeutic efficacy of quercetin-loaded polymeric nanoparticles on triple-negative breast cancer by inhibiting uPA. *RSC Advances* **2020**, *10*, 34517-34526, http://dx.doi.org/10.1039/D0RA04231E.
45. Mohammed, H.A.; Sulaiman, G.M.; Anwar, S.S.; Tawfeeq, A.T.; Khan, R.A.; Mohammed, S.A.; Al-Omar, M.S.; Alsharidah, M.; Rugaie, O.A.; Al-Amiery, A.A. Quercetin against MCF7 and CAL51 breast cancer cell lines: apoptosis, gene expression and cytotoxicity of nano-quercetin. *Nanomedicine* **2021**, *16*, 1937-1961, http://dx.doi.org/10.2217/nnm-2021-0070.
46. Yadav, N.; Tripathi, A.K.; Parveen, A. PLGA-Quercetin Nano-Formulation Inhibits Cancer Progression via Mitochondrial Dependent Caspase-3, 7 and Independent FoxO1 Activation with Concomitant PI3K/AKT Suppression. *Pharmaceutics* **2022**, *14*, 1326, http://dx.doi.org/10.3390/pharmaceutics14071326.
47. Pandya, N.B.; Tigari, P.; Dupadahalli, K.; Kamurthy, H.; Nadendla, R.R. Antitumor and antioxidant status of Terminalia catappa against Ehrlich ascites carcinoma in Swiss albino mice. *Indian journal of pharmacology* **2013**, *45*, 464, http://dx.doi.org/10.4103/0253-7613.117754.

48. Granado-Serrano, A.B.; Martín, M.A.; Bravo, L.; Goya, L.; Ramos, S. Quercetin modulates Nrf2 and glutathione-related defenses in HepG2 cells: Involvement of p38. *Chemico-Biological Interactions* **2012**, *195*, 154-164, http://dx.doi.org/10.1016/j.cbi.2011.12.005.
49. Xu, D.; Hu, M.-J.; Wang, Y.-Q.; Cui, Y.-L. Antioxidant activities of quercetin and its complexes for medicinal application. *Molecules* **2019**, *24*, 1123, http://dx.doi.org/10.3390/molecules24061123.
50. Alam, M.M.; Abdullah, K.; Singh, B.R.; Naqvi, A.H.; Naseem, I. Ameliorative effect of quercetin nanorods on diabetic mice: mechanistic and therapeutic strategies. *RSC advances* **2016**, *6*, 55092-55103, http://dx.doi.org/10.1039/C6RA04821H.
51. Lesjak, M.; Beara, I.; Simin, N.; Pintać, D.; Majkić, T.; Bekvalac, K.; Orčić, D.; Mimica-Dukić, N. Antioxidant and anti-inflammatory activities of quercetin and its derivatives. *Journal of Functional Foods* **2018**, *40*, 68-75, http://dx.doi.org/10.1016/j.jff.2017.10.047.
52. Yilmaz, S.; Alpa, Ş; Nisari, M.; Karatoprak, G.Ş.; Doğanyiğit, Z.; Ülger, H.; Ertekin, T. Examining the antitumoral effect of cornelian cherry Cornus mas in ehrlich ascites tumor-induced mice. *Journal of the Anatomical Society of India* **2019**, *68*, 16-22, https://doi.org/10.4103/jasi.Jasi_28_19.
53. Yılmaz, S.; Ülger, H.; Ertekin, T.; Yay, A.H.; Nisari, M.; Alpa, Ş.; Acer, N. Investigating the anti-tumoral effect of curcumin on the mice in which Ehrlich ascites and solid tumor is created. *Iran J Basic Med Sci* **2019**, *22*, 418-425, http://dx.doi.org/10.22038/ijbms.2019.33623.8019.
54. Yilmaz, S.; Aslan, E.; Doganyigit, Z. Detection of antitumoral effects of quercetin through protein synthesis associated with argyrophilic nucleolar-regulating region. *Hum Exp Toxicol* **2021**, *40*, 90-99, http://dx.doi.org/10.1177/0960327120943916.
55. Tousson, E.; Hafez, E.; Abo Gazia, M.M.; Salem, S.B.; Mutar, T.F. Hepatic ameliorative role of vitamin B17 against Ehrlich ascites carcinoma-induced liver toxicity. *Environ Sci Pollut Res Int* **2020**, *27*, 9236-9246, http://dx.doi.org/10.1007/s11356-019-06528-6.
56. Abd Eldaim, M.A.; Tousson, E.; El Sayed, I.E.T.; Abd Elmaksoud, A.Z.; Ahmed, A.A. Ameliorative effects of 9-diaminoacridine derivative against Ehrlich ascites carcinoma–induced hepatorenal injury in mice. *Environmental Science and Pollution Research* **2021**, *28*, 21835-21850, http://dx.doi.org/10.1007/s11356-020-11857-y.
57. Medhat, D.; Hussein, J.; El-Naggar, M.E.; Attia, M.F.; Anwar, M.; Latif, Y.A.; Booles, H.F.; Morsy, S.; Farrag, A.R.; Khalil, W.K.B.; *et al*. Effect of Au-dextran NPs as antitumor agent against EAC and solid tumor in mice by biochemical evaluations and histopathological investigations. *Biomed Pharmacother* **2017**, *91*, 1006-1016, http://dx.doi.org/10.1016/j.biopha.2017.05.043.
58. Sanchez-Gonzalez, P.D.; Lopez-Hernandez, F.J.; Duenas, M.; Prieto, M.; Sanchez-Lopez, E.; Thomale, J.; Ruiz-Ortega, M.; Lopez-Novoa, J.M.; Morales, A.I. Differential effect of quercetin on cisplatin-induced toxicity in kidney and tumor tissues. *Food Chem Toxicol* **2017**, *107*, 226-236, http://dx.doi.org/10.1016/j.fct.2017.06.047.
59. Min, K.; Ebeler, S.E. Flavonoid effects on DNA oxidation at low concentrations relevant to physiological levels. *Food Chem Toxicol* **2008**, *46*, 96-104, http://dx.doi.org/10.1016/j.fct.2007.07.002.
60. Russo, M.; Spagnuolo, C.; Tedesco, I.; Bilotto, S.; Russo, G.L. The flavonoid quercetin in disease prevention and therapy: facts and fancies. *Biochem Pharmacol* **2012**, *83*, 6-15, http://dx.doi.org/10.1016/j.bcp.2011.08.010.
61. Moon, J.H.; Nakata, R.; Oshima, S.; Inakuma, T.; Terao, J. Accumulation of quercetin conjugates in blood plasma after the short-term ingestion of onion by women. *Am J Physiol Regul Integr Comp Physiol* **2000**, *279*, R461-467, http://dx.doi.org/10.1152/ajpregu.2000.279.2.R461.
62. Farag, M.R.; Moselhy, A.A.A.; El-Mleeh, A.; Aljuaydi, S.H.; Ismail, T.A.; Di Cerbo, A.; Crescenzo, G.; Abou-Zeid, S.M. Quercetin Alleviates the Immunotoxic Impact Mediated by Oxidative Stress and Inflammation Induced by Doxorubicin Exposure in Rats. *Antioxidants (Basel)* **2021**, *10*, http://dx.doi.org/10.3390/antiox10121906.
63. Batista, A.P.; da Silva, T.G.; Teixeira, A.A.; de Medeiros, P.L.; Teixeira, V.W.; Alves, L.C.; dos Santos, F.A. Melatonin effect on the ultrastructure of Ehrlich ascites tumor cells, lifetime and histopathology in Swiss mice. *Life Sci* **2013**, *93*, 882-888. http://dx.doi.org/10.1016/j.lfs.2013.10.012.
64. Raju, A.B.; Y, V.G.; A, R.; G, K.; V, P.R. Antitumor Activity of Diospyros peregrina on Ehrlich Ascites Carcinoma in Mice. *Journal of Scientific Research* **2011**, *3*, 413-419, http://dx.doi.org/10.3329/jsr.v3i2.6787.
65. Tuli, H.S.; Sandhu, S.S.; Sharma, A.K. Pharmacological and therapeutic potential of Cordyceps with special reference to Cordycepin. *3 Biotech* **2014**, *4*, 1-12, http://dx.doi.org/10.1007/s13205-013-0121-9.

66. Russo, M.; Palumbo, R.; Tedesco, I.; Mazzarella, G.; Russo, P.; Iacomino, G.; Russo, G.L. Quercetin and anti-CD95(Fas/Apo1) enhance apoptosis in HPB-ALL cell line. *FEBS Lett* **1999**, *462*, 322-328, http://dx.doi.org/10.1016/s0014-5793(99)01544-6.
67. Aalinkeel, R.; Bindukumar, B.; Reynolds, J.L.; Sykes, D.E.; Mahajan, S.D.; Chadha, K.C.; Schwartz, S.A. The dietary bioflavonoid, quercetin, selectively induces apoptosis of prostate cancer cells by down-regulating the expression of heat shock protein 90. *Prostate* **2008**, *68*, 1773-1789, http://dx.doi.org/10.1002/pros.20845.
68. Tan, J.; Wang, B.; Zhu, L. Regulation of survivin and Bcl-2 in HepG2 cell apoptosis induced by quercetin. *Chem Biodivers* **2009**, *6*, 1101-1110, http://dx.doi.org/10.1002/cbdv.200800141.
69. Zhang, Q.; Zhao, X.H.; Wang, Z.J. Flavones and flavonols exert cytotoxic effects on a human oesophageal adenocarcinoma cell line (OE33) by causing G2/M arrest and inducing apoptosis. *Food Chem Toxicol* **2008**, *46*, 2042-2053, http://dx.doi.org/10.1016/j.fct.2008.01.049.
70. Zhang, Q.; Zhao, X.H.; Wang, Z.J. Cytotoxicity of flavones and flavonols to a human esophageal squamous cell carcinoma cell line (KYSE-510) by induction of G2/M arrest and apoptosis. *Toxicol In vitro* **2009**, *23*, 797-807, http://dx.doi.org/10.1016/j.tiv.2009.04.007.
71. Franco, J.L.; Braga, H.C.; Stringari, J.; Missau, F.C.; Posser, T.; Mendes, B.G.; Leal, R.B.; Santos, A.R.; Dafre, A.L.; Pizzolatti, M.G.; *et al*. Mercurial-induced hydrogen peroxide generation in mouse brain mitochondria: protective effects of quercetin. *Chem Res Toxicol* **2007**, *20*, 1919-1926, http://dx.doi.org/10.1021/tx7002323.
72. Rather, R.A.; Bhagat, M. Quercetin as an innovative therapeutic tool for cancer chemoprevention: Molecular mechanisms and implications in human health. *Cancer medicine* **2020**, *9*, 9181-9192, http://dx.doi.org/10.1002/cam4.1411.
73. Ren, K.-W.; Li, Y.-H.; Wu, G.; Ren, J.-Z.; Lu, H.-B.; Li, Z.-M.; Han, X.-W. Quercetin nanoparticles display antitumor activity via proliferation inhibition and apoptosis induction in liver cancer cells. *International journal of oncology* **2017**, *50*, 1299-1311, http://dx.doi.org/10.3892/ijo.2017.3886.
74. Yu, D.; Ye, T.; Xiang, Y.; Shi, Z.; Zhang, J.; Lou, B.; Zhang, F.; Chen, B.; Zhou, M. Quercetin inhibits epithelial–mesenchymal transition, decreases invasiveness and metastasis, and reverses IL-6 induced epithelial–mesenchymal transition, expression of MMP by inhibiting STAT3 signaling in pancreatic cancer cells. *OncoTargets and therapy* **2017**, *10*, 4719, http://dx.doi.org/10.2147/OTT.S136840.
75. Wu, L.; Li, J.; Liu, T.; Li, S.; Feng, J.; Yu, Q.; Zhang, J.; Chen, J.; Zhou, Y.; Ji, J. Quercetin shows antitumor effect in hepatocellular carcinoma LM3 cells by abrogating JAK2/STAT3 signaling pathway. *Cancer medicine* **2019**, *8*, 4806-4820, http://dx.doi.org/10.1002/cam4.2388.
76. Song, W.; Zhao, X.; Xu, J.; Zhang, H. Quercetin inhibits angiogenesis-mediated human retinoblastoma growth by targeting vascular endothelial growth factor receptor. *Oncology Letters* **2017**, *14*, 3343-3348, http://dx.doi.org/10.3892/ol.2017.6623.
77. Liu, Y.; Li, C.-L.; Xu, Q.-Q.; Cheng, D.; Liu, K.-D.; Sun, Z.-Q. Quercetin inhibits invasion and angiogenesis of esophageal cancer cells. *Pathology-Research and Practice* **2021**, *222*, 153455, http://dx.doi.org/10.1016/j.prp.2021.153455.
78. Liu, K.C.; Yen, C.Y.; Wu, R.S.; Yang, J.S.; Lu, H.F.; Lu, K.W.; Lo, C.; Chen, H.Y.; Tang, N.Y.; Wu, C.C.; *et al*. The roles of endoplasmic reticulum stress and mitochondrial apoptotic signaling pathway in quercetin-mediated cell death of human prostate cancer PC-3 cells. *Environ Toxicol* **2014**, *29*, 428-439, http://dx.doi.org/10.1002/tox.21769.
79. Banerjee, T.; Van der Vliet, A.; Ziboh, V.A. Downregulation of COX-2 and iNOS by amentoflavone and quercetin in A549 human lung adenocarcinoma cell line. *Prostaglandins Leukot Essent Fatty Acids* **2002**, *66*, 485-492, http://dx.doi.org/10.1054/plef.2002.0387.
80. Roos, W.P.; Kaina, B. DNA damage-induced cell death by apoptosis. *Trends Mol Med* **2006**, *12*, 440-450, http://dx.doi.org/10.1016/j.molmed.2006.07.007.
81. Granado-Serrano, A.B.; Martín, M.A.; Bravo, L.; Goya, L.; Ramos, S. Quercetin induces apoptosis via caspase activation, regulation of Bcl-2, and inhibition of PI-3-kinase/Akt and ERK pathways in a human hepatoma cell line (HepG2). *The Journal of nutrition* **2006**, *136*, 2715-2721, http://dx.doi.org/10.1093/jn/136.11.2715.

Supplementary materials

Table S1. The primer sequences used for qRT-PCR analysis.

Gene	Sequence	Accession number
VEGF	F: 5`-GTACCTCCACCATGCCAAGT-3` R: 5`-TCACATCTGCAAGTACGTTCG- 3`	NM_001025257.3
β-actin	F:5`-GGGAAATCGTGCGTGACAT-3 R: 5′-GCGGCAGTGGCCATCTC-3′	NM_007393.5

Table S2. Hematological parameters in EAC-bearing mice treated with QUR or QURnp.

Parameters	Groups						
	EAC	QUR 10mg/kg	QUR 25mg/kg	QUR 50mg/kg	QURnp 10mg/kg	QURnp 25mg/kg	QURnp 50mg/kg
Hb content (g%)	8.4±0.6	9.7±0.4	10.6±0.28*	11.3±0.39*	11.7±0.36*	11.9±0.2*	12.8±0.2*
RBC (cells $\times 10^6/mm^3$)	3.1±0.45	4.7±0.5	5.1±0.35*	4.7±0.16*	4.9±0.51*	5.4±0.3*	5.6±0.42*
WBC (cells $\times 10^3/mm^3$)	12.9±0.32	10.3±0.45*	9±0.37*	8.8±0.2*	8.1±0.25*	7.71±0.24*	7.6±0.19*

* Significant compared with EAC inoculated mice control group $p < 0.05$, Data are presented as mean ± SE. EAC: Ehrlich ascites carcinoma; SE: Standard error; QUR: Quercetin; QURnp: QUR-loaded Pluronic nanoparticles.